



Contents lists available at ScienceDirect

Journal of Molecular Liquids

journal homepage: www.elsevier.com/locate/molliq

Colloidal nanomedicines with prolonged release of chloroquine based on interactions with aromatic polymers after mixing two liquids: from in silico simulation of nanoparticle formation to efficient in-bench scale up

María Gabriela Villamizar-Sarmiento^{a,b,*}, Osvaldo Yáñez^{c,d,*}, Mario E. Flores^g, Gonzalo Álvarez-Acevedo^{a,b}, Fernando González-Nilo^e, Juan Guerrero^f, Ignacio Moreno-Villoslada^{g,*}, Felipe A. Oyarzun-Ampuero^{a,b,c,*}

^a Department of Sciences and Pharmaceutical Technology, University of Chile, Santiago de Chile 8380494, Chile

^b Advanced Center for Chronic Diseases (ACCDiS), Santiago 8380494, Chile

^c Center of New Drugs for Hypertension (CENDHY), Universidad de Chile & Pontificia Universidad Católica de Chile, Santiago, Chile

^d Núcleo de Investigación en Data Science, Facultad de Ingeniería y Negocios, Universidad de las Américas, Santiago 7500000, Chile

^e Center for Bioinformatics and Integrative Biology (CBIB), Facultad de Ciencias de la Vida, Universidad Andres Bello, Av. República 330, Santiago 8370146, Chile

^f Laboratorio de Compuestos de Coordinación y Química Supramolecular, Facultad de Química y Biología, Universidad de Santiago de Chile, Av. Libertador Bernardo O'Higgins 3363, Estación central, 9170002 Santiago, Chile

^g Laboratorio de Polímeros, Instituto de Ciencias Químicas, Facultad de Ciencias, Universidad Austral de Chile. Valdivia 5090000, Chile

ARTICLE INFO

Keywords:

Chloroquine
Aromatic-aromatic interactions
Aromatic polyelectrolytes
Nanoparticles
Drug delivery
Prolonged release

ABSTRACT

Nanomedicines containing the aromatic drug chloroquine and the polymer poly(sodium 4-styrenesulfonate) have been theoretically designed and experimentally synthesized following the simple mixture of two aqueous solutions containing the drug and the polymer, respectively. Theoretical calculations show higher binding energy between both the aromatic polymer and chloroquine, and a higher tendency to release water from their hydration spheres, as compared to the binding between the drug and the aliphatic polymer poly(sodium vinyl sulfonate). MD simulations show the spontaneous formation of stable structures of 10 nm of average diameter, even combining short polymer chains, highly diluted reactants, and short reaction time (in the range of μ s). Rapid mixture of the liquids in a stopped flow equipment shows nanoparticle formation in the range of tenths of seconds. Equilibration studies in the range of minutes evidence spheroidal nanoparticles with almost quantitative association efficiency, 48.6 % of drug loading, size of 170 – 410 nm, low polydispersity ($PdI = 0.25 - 0.47$), and negative zeta potential ($-18 - -45$ mV). They provide drug release for 30 days, and are stable to NaCl exposure, pH gradient, several temperature values, and long-term storage. Furthermore, we demonstrate scaling up of the nanomedicine production upon increasing the reaction volume. Our studies demonstrate that these highly loaded drug nanoparticles are based on the occurrence of site-specific short-range interactions between the drug and the aromatic excipient such as π -stacking. In the absence of the aromatic group in the polymer, weak interactions and unstable formulations are evidenced, both theoretically and experimentally. The combination of the selected theoretical and experimental tools could promote the efficient production of drug / polyelectrolyte formulations with therapeutical applications. The chosen components could be considered as potential medicines or as model components to design, develop, characterize, and scale up medicines comprising other combinations of drugs and polymers.

* Corresponding authors.

E-mail addresses: mvillamizar@postqyf.uchile.cl (M. Gabriela Villamizar-Sarmiento), oyanez@udla.cl (O. Yáñez), mario.flores@uach.cl (M.E. Flores), gongaalvarez@um.uchile.cl (G. Álvarez-Acevedo), fernando.gonzalez@unab.cl (F. González-Nilo), juan.guerrero@usach.cl (J. Guerrero), imorenvilloslada@uach.cl (I. Moreno-Villoslada), foyarzuna@ciq.uchile.cl (F.A. Oyarzun-Ampuero).

¹ These authors contributed equally to this work.

<https://doi.org/10.1016/j.molliq.2023.123906>

Received 29 August 2023; Received in revised form 3 December 2023; Accepted 23 December 2023

Available online 30 December 2023

0167-7322/© 2023 Elsevier B.V. All rights reserved.

1. Introduction

Polymeric drug delivery systems in the form of nanoparticles (NPs) are advantageous for controlled administration of drugs into the body, helping to achieve desired target tissues, prolonging drug release, and providing stable drug concentration in blood, without imposing strict schedules of medicine administration to patients [1–5]. Among the different drugs, it deserves special attention the vast number of active molecules accomplishing these four requisites: possessing aromatic residues, bearing ionizable groups, showing low molecular-weight (≤ 500 Da), and being water-soluble [6,7]. Following traditional nanoencapsulation strategies, these drugs are difficult to encapsulate [8–10].

Interestingly, this kind of drugs should potentially undergo aromatic-aromatic interactions with aromatic excipients such as aromatic polymers. In particular, with the aid of aromatic polyelectrolytes oppositely charged with respect to several drugs, NPs with outstanding drug loading of around 50 % could be easily produced making use of a combination of long-range electrostatic interactions and short-range aromatic-aromatic interactions [8–11]. However, robust studies providing a neat image of the formation process of colloidal particles in water upon interaction between aromatic polyelectrolytes and complementary charged aromatic drugs are still missed, as well as the estimation of the energy involved. Short-range aromatic-aromatic interactions in water between oppositely charged groups are conceived to involve long-range electrostatic interaction, a strong hydrophobic contribution, short-range electrostatic interactions, and may be potentially complemented with van der Waals interactions and hydrogen bonding [12–14].

Chloroquine (CQ) is an interesting drug to be nanoencapsulated due to the variety of chronic diseases where this drug is currently used (rheumatoid arthritis, systemic lupus erythematosus, spondylitis, and rosacea, among others) [15–19] and/or under investigation (cancer, diabetes, atherosclerosis, dermatomyositis, and Sjögren's syndrome, among others) [20–25]. The prevention of important side effects occurring with conventional formulations containing CQ (such as retinopathy, cardiomyopathy, myopathy, and neuromyopathy) can be supported with the development of stable nanoformulations able to supply prolonged and controlled release [18]. Importantly, CQ is an aromatic dicationic drug comprising a quinoline ring and other protonable amines in aliphatic residues: the high positive charge, the extension of its π cloud, and the extension of its flexible aliphatic moiety may allow strong interaction with aromatic polymers, with several binding sites. Thus, providing a robust study of the interaction of CQ with aromatic polymeric species, as well as the collapse of the system as a colloidal suspension, both theoretically and experimentally, is of major importance to understand the behaviour and dynamics of nanomedicines based on this and similar drug species.

To study non-covalent interactions between drugs and polymers, able to sustain a colloidal state, the non-covalent interactions (NCI) plot in density functional theory (DFT) serves as a powerful visualization technique, offering a comprehensive means to analyze and identify non-covalent interactions within molecules and materials [26–31]. This method relies on the reduced density gradient (s) and electron density (ρ) to pinpoint regions characterized by low s and low ρ , indicative of non-covalent interactions such as hydrogen bonds and van der Waals forces. The strength and nature of these interactions can be further characterized by examining the sign and magnitude of the second eigenvalue (λ_2) of the electron density Hessian matrix. One of the notable features of the NCI plot is its ability to visualize non-covalent interactions in three-dimensional space. The color-coded representation, based on the strength and type of interaction, enhances the interpretability of the plot. Moreover, this technique is versatile, applicable to both wavefunction calculations from quantum chemistry methods like DFT and experimental electron densities obtained from X-ray diffraction. Importantly, the NCI remains invariant to transformations of molecular orbitals, providing a real-space representation of non-

covalent interactions. Analysis tools, such as the integration of density over interaction strength ranges, enable the quantification of the relative strength of interactions. Consequently, the NCI plot serves as a valuable tool for gaining insights into diverse aspects of molecular behavior, including chemical bonding, intermolecular forces, molecular packing, and protein–ligand binding. The utility of the NCI plot extends beyond qualitative visualization. It also facilitates a quantitative understanding of weak interactions that influence the structure, function, and properties of molecules.

In this work, we will study the interaction, after the mixture of two aqueous liquids, of the drug CQ with the Food and Drug Administration (FDA) approved polymer poly(sodium 4-styrenesulfonate) (PSS) [32–37], focusing at producing high loading drug nanoparticles (HLDNPs), demonstrating in-bench scale-up and prolonged drug release. Several quantum chemical calculations and molecular dynamics (MD) tools will be applied to the combination of the components in order to calculate the involved binding energy, involved interacting groups, and the dynamic behaviour of the reactants. Control experiments (for theoretical and experimental analysis) will be done with the non-aromatic polyelectrolyte poly(sodium vinylsulfonate) (PVS). The nature of the interactions between components and the obtained structures are presented and discussed. Furthermore, important pharmaceutical parameters such as association efficiency (AE), drug loading (DL), stability in several conditions (NaCl exposure, pH gradient, temperatures, and long-term storage), and drug release profiles are analysed and discussed for the obtained HLDNPs. The combination of the selected theoretical and experimental tools could promote the efficient production of drug / polyelectrolyte formulations with therapeutical applications.

2. Materials and methods

2.1. Materials

Chloroquine diphosphate (CQ, 515.9 g/mol) was purchased from Sigma Aldrich (USA) and used as received. The anionic aromatic polymer PSS (206.2 g/mol of monomeric units) was purchased from Sigma Aldrich (USA), purified and later fractionated over a membrane of a molecular weight cut-off (MWCO) of 5000 Da (Biomax, 63.5 mm diameter) by diafiltration, first with 0.15 M of NaNO_3 (Sigma Aldrich, USA) and later in the absence of NaNO_3 . The anionic aliphatic polymer poly(sodium vinylsulfonate) (PVS) (130.1 g/mol of monomeric units) was purchased from Sigma Aldrich (USA) and used as received. The pH was controlled with an Edge® HI2002 pH meter (Hanna Instruments, USA) using minimum amounts of NaOH and HCl (Merck, Germany). For the stability experiments, the ionic strength was reached using different concentrations of sodium chloride, NaCl (Sigma Aldrich, USA). All the solutions were prepared with Milli-Q water obtained from a Simplicity SIMS 00001 equipment (Millipore, France), except to the NMR experiments where the solutions were prepared with deuterium-depleted water, D_2O (Sigma Aldrich, USA). The chemical structures of CQ and each polymer (PSS and PVS) are shown in Fig. S1.

2.2. Methods

2.2.1. Theoretical methodology

2.2.1.1. Intermolecular interaction energy. The local and global minimum for 10 000 interacting species, including CQ and polymer (PSS or PVS), were explored with the SnippetKick algorithm [38–43], which uses a stochastic method. This is an implementation of the Kick algorithm [44–46]. The Kick algorithm is designed to search for the putative global minimum in molecules of a desired chemical composition, as well as complex systems such as the CQ / polymer systems. The geometry optimizations were carried out using the PM6-D3H4 [47] semi-

empirical quantum–mechanical method implemented in MOPAC16 [48] and using the COSMO solvent model. The lowest energy isomer reported by the searches was used for intermolecular interaction energy calculations.

The strategy for calculating the intermolecular interaction energy of CQ in the presence of PSS and PVS is as follows: each fragment of the system was considered separately, these fragments being the CQ molecule, PSS, and PVS polymer chain. Each one was optimized separately using the PM6-D3H4 semi-empirical quantum–mechanical method and solvation effects were included via the COSMO model. Furthermore, each of these fragments was re-optimised with the Density-Functional Theory (DFT) by a hybrid functional PBE0 [49] (Perdew–Burke–Ernzerhof exchange energy and Hartree–Fock exchange energy) with 6-31G* basis set and the Grimme dispersion correction (D3) [50]. Water was simulated as a solvent using the SMD parametrization of the IEF-PCM [51]. The DFT quantum mechanics calculations were performed using the Gaussian16 software [52]. Subsequently, the heat of formation (ΔH_f°) and energies (E) were calculated for each fragment using PM6-D3H4//COSMO and PBE0-D3/6-31G*//PCM. Finally, the intermolecular interaction energy (ΔE_{bind}) was obtained according to the following equations:

$$\Delta E_{bind}^{PM6-D3H4} = \Delta H_{f_{polymer+CQ}}^\circ - (\Delta H_{f_{polymer}}^\circ + \Delta H_{f_{CQ}}^\circ) \quad (1)$$

$$\Delta E_{bind}^{PBE0-D3/6-31G^*} = E_{polymer+CQ} - (E_{polymer} + E_{CQ}) \quad (2)$$

2.2.1.2. Noncovalent interaction index (NCI). To reveal possible non-covalent CQ interactions in the presence of PSS and PVS, such as hydrogen bonds, π -stacking, anion- π interactions, steric repulsion, and van der Waals interactions, we used the non-covalent interaction index (NCI) [28,29]. The NCI is based on the electron density (ρ), its derivatives, and the reduced density gradient (s). In this work, all these calculations were carried out with PBE0-D3/6-31G*. Water was simulated as a solvent using the SMD parametrization of the IEF-PCM [51]. The quantum mechanics calculations were performed using the Gaussian16 software [52]. The NCI was computed using the GPUAM [53] and NCIplot [28] softwares. Molecular visualization of the systems was carried out with the VMD software package [54].

2.2.1.3. All-atom molecular dynamics simulations. Classical MD simulations were performed using the package NAMD-GPU 3.0 software [55]. Four MD simulations were performed for the species shown in Table S1 interacting in aqueous medium. Chloroquine (CQ) dication was parametrized using the LigParGen web server (<http://zarbi.chem.yale.edu/ligpargen/>) and implementing the OPLS-AA/1.14*CM1A(-LBCC) force field parameters for organic ligands [56,57]. The polymeric model of PSS and PVS used the CHARMM22 protein force field [58] and Merck molecular force field [59]. The specific parameters used for the molecular simulations can be found in the Supplementary Material. The simulations were carried out using the CHARMM27 force field in an explicit solvent with the TIP3P water model ($\approx 44\,000$ water molecules). Starting configurations were generated in cubic boxes with lateral dimensions of $120 \times 120 \times 100 \text{ \AA}^3$. The systems were prepared by randomly placing CQ, PSS or PVS, and water molecules in the simulation box using the Packmol software [60], that creates an initial point for MD simulations by packing molecules in defined regions of space. First, each system was minimized until convergence (40 000 steps) was reached and then was equilibrated by 1 ns. Then, 200-ns-long production MD simulations were performed on each system. During the MD simulations, the equations of motion were integrated with a 2.0 fs time step in the NPs ensemble. The SHAKE algorithm was applied for all hydrogen atoms, and the van der Waals cutoff was set to 10.0 \AA . The temperature was maintained at 300 K by employing the Nose-Hoover thermostat method with a relaxation time of 1.0 ps. The Langevin piston Nose-Hoover method was used to control the pressure at 1.0 atm. Long-range electrostatic interactions were considered by means of the

particle mesh Ewald approach. Data were collected every 50 ps during the MD runs. Molecular visualization of the systems and MD trajectory analysis were carried out with the VMD software package [54].

2.2.1.4. Coarse-grained molecular dynamics simulations. The process of coarse graining involves reducing the degree of freedom by representing the group of atoms by a bead. In this work, we have used PSS polymer and CQ molecule coarse grained (CG) based on the MARTINI model [61]. In general, the MARTINI model maps four heavy atoms (excluding hydrogen) to a single bead, while for structures containing ring, two or three atoms are mapped to a bead. There are four main types of interaction sites: polar (P), non-polar (N), apolar (C), and charged (Q). Each main type is further divided into subtypes depending on its hydrogen bonding capabilities as donor (d), acceptor (a), both (da), and none (0), or by a number denoting a degree of polarity from high (5) to low (1). The PSS polymer MARTINI CG models are based on the CG model developed by Yethiraj et al. [62,63]. In this model each monomer (4-styrene sulfonate) group consists of five CG sites. The CG bead for the backbone is assigned as type SC1 such that its center of mass is in between two consecutive styrene groups. SC4 is assigned for the ring bead, Qa for the sulfonate group, and Qd for the sodium counterion (the SC1, SC4, Qa, and Qd types are the standard MARTINI particle types). The CG mapping structure and parameters were carried out with Auto_MARTINI in the case of CQ dication [64,65]. The system was then solvated using $\sim 10^5$ MARTINI water molecules (four water molecules are mapped to one CG water bead).

After energy-minimization (40 000 steps) of the CG system, the simulation was equilibrated for 300 ns before a 6.5- μ s production run using the package NAMD-GPU 3.0 software [55]. The temperature was kept at 300 K using a Langevin thermostat with a damping coefficient of 0.5 ps. Periodic boundary conditions (PBC) were used and the pressure was kept at 1 atm using a Nose-Hoover-Langevin piston [66] with a piston period of 200 fs and a decay time of 100 fs. Non-bonded interactions were cutoff at 12 \AA , with shifting throughout the interaction range for electrostatic interactions and beginning at 9 \AA for van der Waals interactions to implement a smooth cutoff. Pair lists were updated at least once per 10 steps, with a 14 \AA pair list cutoff. The simulations were performed using a 20 fs time step.

2.2.2. Experimental methodology

2.2.2.1. UV-vis and NMR spectroscopy. UV-vis experiments were performed in a spectrophotometer Agilent 8453 (Agilent, USA) using a quartz cuvette (Hellma®, Germany) of 1 cm of path length. Solutions of [CQ] = 2×10^{-5} M in the presence of the polymers ([PSS] = 5×10^{-5} M or [PVS] = 5×10^{-5} M of monomeric units) and in the absence of the polymers were selected for the experiments. NMR studies were performed on an Avance400 (Bruker, USA) in D₂O, using 5 mm diameter glass tubes (volume of solution typically 0.7 mL). ¹H NMR experiments were performed under selected conditions of [CQ] = 1×10^{-3} M and [PSS] = 1×10^{-2} M, each compound was lyophilized (volume of 750 μ L) and D₂O was used for reconstitution before analysis.

2.2.2.2. Preparation of CQ / polymer formulations. 5.0 mL of an aqueous solution containing CQ was added to 5.0 mL of an aqueous solution containing the anionic polymer (PSS or PVS) at pH 7 under continuous stirring (5 min). The final apparent concentration was defined in order to obtain different CQ / polymer molar ratios. The final CQ concentration was varied between 3.3×10^{-4} M and 4.0×10^{-3} M and the concentration of the anionic polymer was maintained at 3.3×10^{-3} M. Dynamic light scattering (DLS) was selected to identify (or not) the NPs formation. For scaling up, a selected formulation was tested (CQ / PSS = 0.4). Briefly, the volume of each component (CQ and PSS) was increased by 2.5, 5, and 10 times (before mixing), maintaining the original concentrations to secure the CQ / PSS molar ratio, and, in consequence, the

NPs formation. The obtained formulations were stirred for 5 min at room temperature and pH 7.

2.2.2.3. Nanoparticle characterization. Dynamic light scattering (DLS) and laser Doppler anemometry (LDA) was used to determine the hydrodynamic diameter (including the polydispersity index, PDI) and zeta potential of the NPs, using a ZetaSizer NanoZS (Malvern Instruments, UK). The determination of nanoparticle concentration was performed by Nanoparticle Tracking Analyses (NTA) in a NanoSight NS300 (Malvern Instruments, UK). The formulations were diluted (up to 100 times with Milli-Q water) to reach optimum range of NPs ($10^7 - 10^9$ NPs/mL). At least five videos (one minute each) of the NPs formulation were obtained by the NanoSight. Size distribution and particle concentration were obtained after the analyses of the videos (NTA v 3.0 software, Malvern, UK). Scanning transmission electron microscope (STEM, Inspect F-50, FEI, Holland) was used for the morphological characterization of the NPs. The samples for STEM analyses were obtained sticking a droplet (20 μ L) of the NPs formulation over a grid (copper covered with Formvar, 200 mesh,) during 2 min, later the remotion of the droplet was done with filter paper (avoiding the paper touching the grid), then the grid was washed twice with a droplet of Milli-Q water (1 min) and removing the droplet with filter paper. The sample was then stained (1 % w/v phosphotungstic acid) by adding to the grid for 2 min a droplet of this solution and removing with filter paper. The grid was dried at room temperature for at least 60 min before analyses.

The formation kinetics of the NPs were analyzed by rapid mixing stopped-flow measurements performed in a SFM3000 stopped-flow instrument (Bio-Logic, France) attached to a PMS250 spectrometer (Bio-Logic, France). A MOS-200 (Bio-Logic, France) was used to irradiate the samples with light at the wavelength of 630 nm. Both PMS250 (Bio-Logic, France) photomultiplier (PMT) and optical fiber MOS200 (Bio-Logic, France) were set at 90°, allowing detection of scattered light. A two phases method was programmed in the stopped-flow software Biokine version 4.6 (Bio-Logic, France), to first wash the cuvette with 75 μ L of water during 100 ms and then mixing, during 25 ms, equal amounts (75 μ L) of PSS 6.6×10^{-3} M and different CQ solutions, respectively, covering a CQ / PSS molar ratio from 0.1 to 0.7. This mixing method has a deadtime of 3.6 ms. The variation of PMT voltage as function of time was monitored up to 100 s with sampling periods of 50 ms. At least 10 replicates were done for each CQ / PSS molar ratio, and the average curve was obtained using the Biokine software. The resulting average data was fitted to the monoexponential function

$$y = at + b + C_1 e^{-k_1 t} \quad (3)$$

as well as to the bioexponential function

$$y = at + b + C_1 e^{-k_1 t} + C_2 e^{-k_2 t} \quad (4)$$

where y corresponds to the scattered light intensity, t is the time (s), a and b are two fitting constants, C_n is the amplitude for the process n , and k_n is the kinetic constant (s^{-1}). The quality of the fit is assessed from the reduced χ^2 error values [67], which is defined as

$$\chi^2 = \frac{1}{N} \sum_{i=1}^N (x_i - \underline{x}_i)^2 \quad (5)$$

In addition, the stability of the formulations was evaluated in terms of hydrodynamic diameter and zeta potential at different stimulus (NaCl exposure, pH gradient, several temperatures, and long-term storage) using a ZetaSizer NanoZS. The concentration of NaCl in the medium was controlled with an automatic titrator (MPT-2, Malvern Instruments, UK). For pH variations, HCl (0.25–0.01 M) and NaOH (0.25–0.01 M) solutions were selected and controlled with the automatic titrator. The temperature of the samples was modified directly in the NanoZS instrument (20–50 °C, with a thermal equilibrium time of 15 min for each measurement of hydrodynamic diameter and zeta potential).

2.2.2.4. Drug association efficiency and drug loading. In order to calculate drug AE and DL, centrifugation / ultrafiltration in Vivaspin®6 tubes (MWCO 3 kDa, 5000 G x 40 min) was selected. Briefly, the AE of CQ in the CQ / PSS formulations was determined analysing the amount of drug in the filtrate so that the amount of drug associated to the polymer over the initial total amount of drug added can be obtained. The DL (% w/w) was calculated by dividing the mass of associated drug by the obtained weight of the formulations. The total weight of the formulations was estimated using different criteria and compared. The criteria were: i) total initial polymeric fraction and associated drug fraction with respective counterions; ii) total initial polymeric fraction and associated drug fraction without respective counterions. CQ quantification was obtained by determining the absorbance at 343 nm (Agilent 8453 spectrophotometer, USA). The standard curve was linear ($R^2 > 0.999$, 4×10^{-5} M to 3×10^{-6} M), the molar extinction coefficient was $14\,577 \text{ M}^{-1} \text{ cm}^{-1}$.

2.2.2.5. In-vitro drug release. In-vitro drug release data were exposed to mathematical kinetics models (program DDSolver) as previously described [68]. The Akaike information criteria (AIC), coefficient of determination (R^2), and the model selection criteria (MSC) values were considered for the selection of the model, then the release data were fitted to different models (zero order, first order, Higuchi, and Korsmeyer-Peppas) [69]. The release data were obtained by conventional dialysis and USP apparatus 4 (continuous flow-cell) as follows:

2.2.2.5.1 Dialysis: CQ / PVS or CQ / PSS formulations (5 mL) were added to a dialysis bag (MWCO 10 kDa, ThermoScientific, USA). The dialysis bag was submerged in Milli-Q water (95 mL, pH 7.0) or conditions simulating biological environments (Milli-Q water, 0.13 M NaCl, pH 7.4), under continuous agitation (C-MAG HS 7, IKA, Staufen, Germany) at 37 °C. The experiments were carried out for 30 days. 500 μ L of the solution were removed at selected time intervals and replaced with the same volume of the release medium. The released CQ was analysed measuring the absorbance of each sample by spectrophotometry (Agilent 8453 spectrophotometer, USA).

2.2.2.5.2 USP apparatus 4: For these experiments, the set-up of the continuous flow method was combined with a dialysis bag containing the NPs into the cell [70]. In brief, CQ / PSS NPs (5 mL) were transferred to the dialysis bag (MWCO 10 kDa, ThermoScientific, USA) and submerged into the flow-cell (12.5 mL capacity). Drug release analyses were evaluated using Milli-Q water (250 mL, pH 7). The continuous flow-cell (Sotax CE 6, Sotax AG, Switzerland) was operated in the close configuration with a flow rate of 4 mL/min at 37 °C. Experiment were carried out during 6 h, 500 μ L of each solution were removed every 15 min and immediately restored with the same volume of Milli-Q water. The released CQ was analysed measuring the absorbance of the aliquots by spectrophotometry (Agilent 8453 spectrophotometer, USA).

3. Results and discussion

3.1. Interactions between CQ and PSS

When aromatic-aromatic interactions are held between an aromatic polyelectrolyte and aromatic counterions, the release of water from the hydration sphere of both interacting groups, together with specific effects associated to the short-range interaction may produce spectroscopic changes, reflected, as seen here, in UV-vis and ^1H NMR spectra. These are differentiating facts with respect to the mere long-range electrostatic interaction. In addition, the resistance to the cleaving effect of added electrolytes in solution is another property associated with aromatic-aromatic interactions whereas a high ionic strength tends to screen long-range electrostatic interactions, which are then cleaved.

The UV-vis spectra of CQ in the absence and in the presence of the aromatic PSS and the non-aromatic polymer PVS (similar to PSS but with the absence of the aromatic ring) used as control are shown in

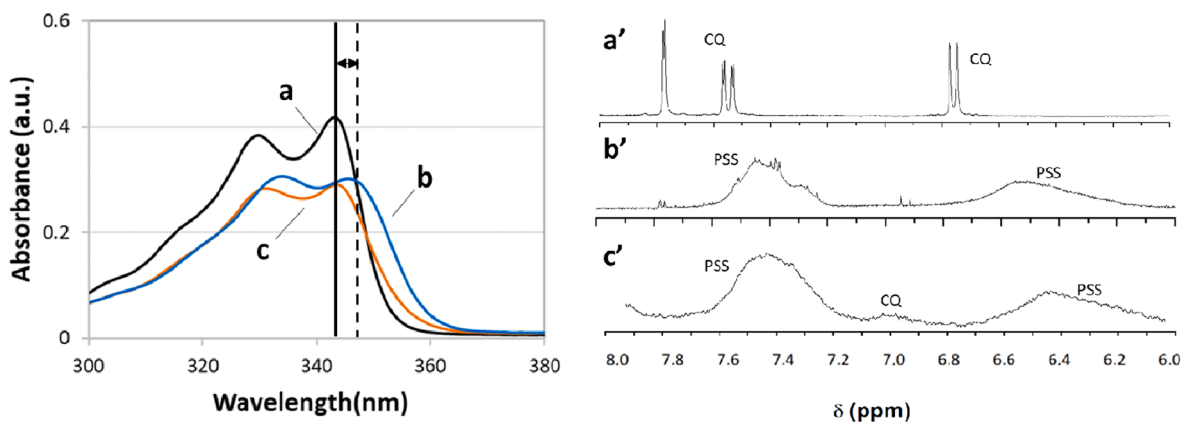


Fig. 1. UV-vis spectra (A) of CQ 2×10^{-5} M pristine (a), in the presence of PSS 5×10^{-5} M (b), and in the presence of PVS 5×10^{-5} M (c). ¹H-NMR spectra (500 MHz) in D₂O at pH 7 of the aromatic region of solutions containing (B): CQ 1×10^{-3} M in the absence of PSS (a'), PSS 1×10^{-2} M (b'), and CQ 1×10^{-3} M in the presence of PSS 1×10^{-2} M (c').

Fig. 1A. Cloudless samples were achieved since the reactants are highly diluted. A bathochromic effect is evident in the CQ spectrum in the presence of PSS that is typical for intimate aromatic-aromatic interactions, as seen for other aromatic counterions [71,72]; this is not observed for CQ in the presence of PVS with which the drug interacts mainly through ionic forces.

The ¹H-NMR spectra of CQ in the presence and in the absence of PSS are shown in Fig. 1B. The signals of the CQ aromatic protons (between 6.0 and 8.0 ppm) are strongly affected by PSS showing upfield shifting and broadening. These features constitute strong evidence of the occurrence of secondary site-specific aromatic-aromatic interactions because the hydration shell of the components changes, and magnetic

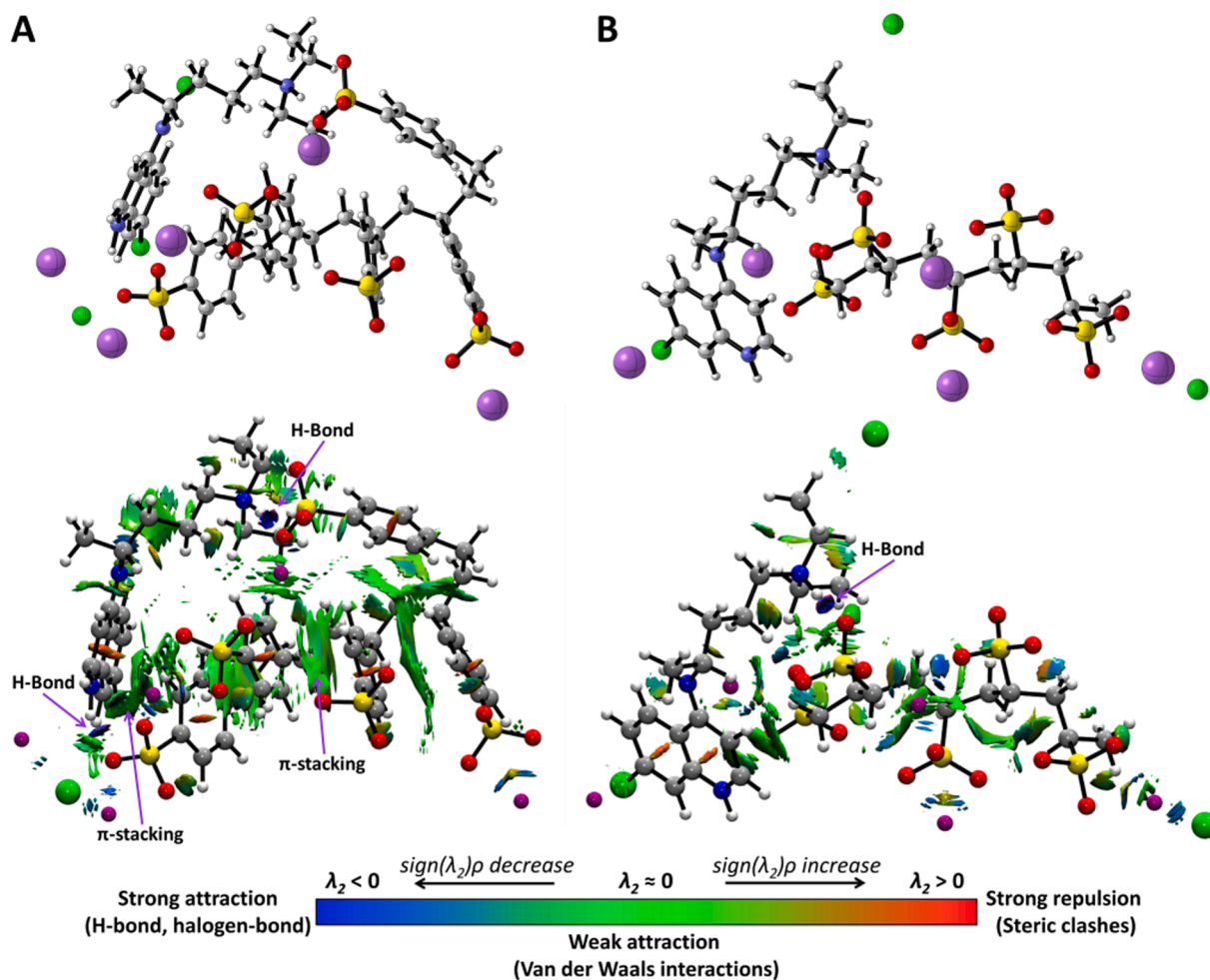


Fig. 2. Non-covalent interactions of (A) CQ + PSS polymer chain and (B) CQ + PVS polymer chain at the lowest energy conformation. The CQ-polymer interactions are illustrated on surfaces, blue indicates strong attractive interactions, green indicates weak interactions, and red indicates overlap interactions. These calculations were performed at the PBE0-D3/6-31G* level of theory.

fields produced by electronic currents of the aromatic groups strongly affect the neighbour structures [8,73–77]. A decrease on the mobility is responsible of the bands broadening and the low signal-to-noise values. In fact, NOESY spectrum as complementary evidence of the short-range interaction could not be acquired due to the low signal-to-noise ratio for the drug proton transitions. This is also interpreted as a sign of the tendency to confine the drug in the polymer domain, thus pointing at the formation of HLDNPs.

Intermolecular interaction energy calculations were used to quantitatively estimate the CQ binding energy to PSS and PVS. Table S2 summarizes the respective binding energy results. The highest binding energies are found for CQ interacting with PVS (-6 – -8 kcal/mol), while very remarkable lower energy values are observed for the CQ / PSS system (-17 – -27 kcal/mol), meaning a higher affinity for the polymer comprising aromatic groups. These intermolecular interaction energies are shown at two levels of theory: PM6-D3H4//COSMO and PBE0-D3/6-31G*/PCM levels. Contributions to the interaction energy between CQ and PSS include hydrogen bonding interaction of the CQ quinoline nitrogen and tertiary amino group with the oxygens of the sulfonate group of each monomer of the PSS chain, as well as the π -stacking interaction between the aromatic quinoline group of CQ and the styrene of the PSS polymer. These contributions are shown in the NCI 3D diagram in Fig. 2. The blue region between quinoline nitrogen and tertiary amino group and the oxygens of the sulfonate group corresponds to hydrogen bonds. These interactions are related to the distance between the O \cdots HN contacts, which is 1.720 Å, for the quinoline nitrogen and the sulfonate oxygens, and 1.831 Å, for the tertiary amino group and sulfonate oxygens. In addition to these non-covalent interactions, there are other attractive interactions, which are represented in green. These interactions are represented by π -stacking and van der Waals forces between the aromatic quinoline group of CQ and the styrene of the PSS polymer.

MD simulations give us trajectories showing interesting features about the CQ interaction with PSS and PVS. Results with only 2 CQ

molecules and 200 monomer units of PSS (CQ / PSS = 0.01) show that CQ tends to bind to the polymer and maintain its binding during the 200 ns trajectory, as can be seen in Fig. S2A. On the contrary, when PVS is present, CQ is observed as free solvated molecules, as can be seen in Fig. S2B. As the concentration of CQ increases in the CQ / PSS system, aggregation of CQ is observed around the PSS polymer chains, forming an interface between the polymer and CQ (Fig. 3), enhancing aggregation.

In Fig. 4A, the radial distribution functions ($g(r)$) clearly show a higher interaction between the quinoline nitrogen atom with the sulfur atom of PSS, compared with PVS, which has a lower probability of interaction with CQ. This is mainly due to the structure of PVS, with no aromatic groups. The solvent accessible surface area (SASA), related with the theoretical available area for the CQ-PSS interaction at the different CQ concentrations (Fig. 4B), show that the area of the polymer increases as the CQ concentration increases, promoting the capture of CQ along the polymer chains. The PSS core is clearly affected by aggregation, and this behaviour is consistent with that observed experimentally. The changes observed when the concentration of CQ increases are associated to changes in the hydrophobicity of the system, driven by a decrease on the amount of water surrounding the PSS polymer due to the mutual CQ / PSS short-range interactions. Strong solvation of ions such as Cl $^-$ and Na $^+$ by water molecules enhances the interaction between CQ and PSS.

To determine the nature of the chemical bonds between CQ and PSS responsible for the stabilization of CQ / PSS HLDNPs, we have analyzed the non-covalent interactions of the most representative cluster of MD trajectories through the promolecular electron densities approach [28,78] (Fig. 5). A polymeric chain of 20 NaSS monomers was taken as a model as the central part at a cutoff distance of 7.0 Å to define the interfacial contact distance. This cutoff distance was centered on the PSS polymer chain, where all CQ molecules at that distance were considered after a previous clustering analysis of the most relevant molecular dynamics. It was found that the most abundant non-covalent interactions

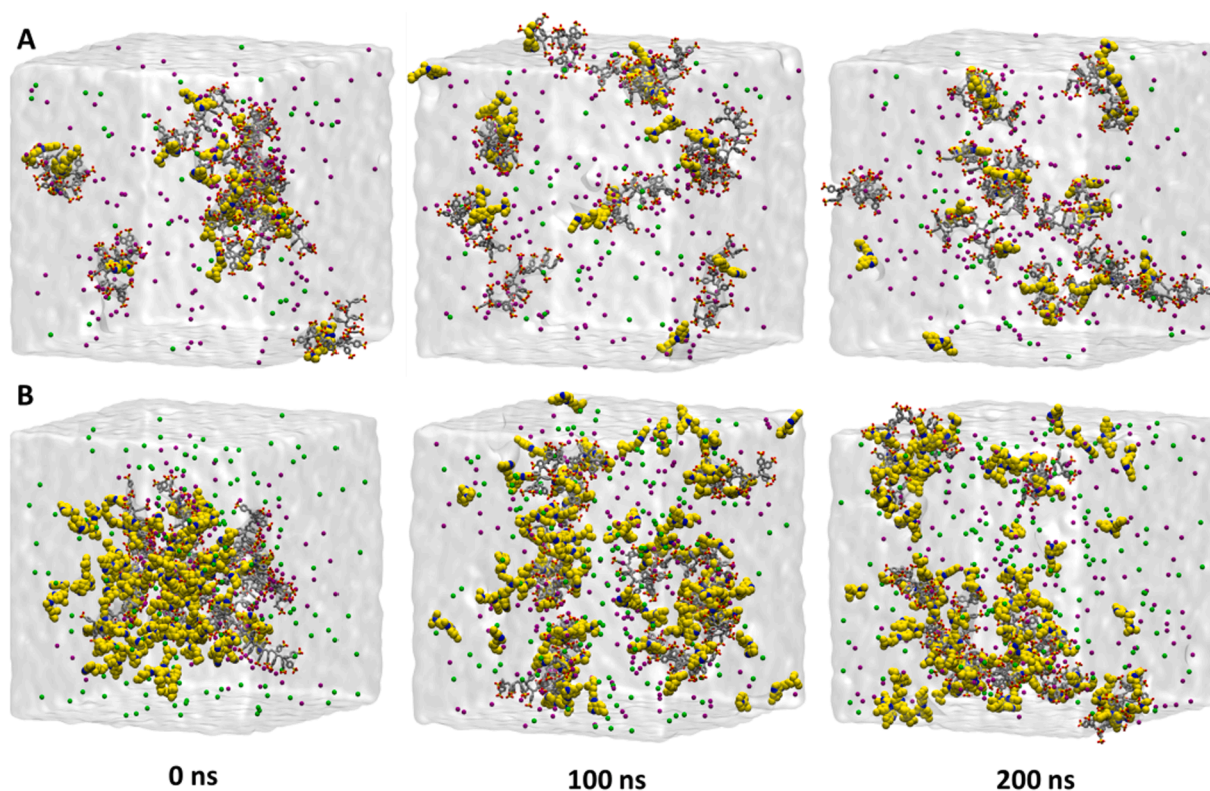


Fig. 3. Trajectory snapshots of PSS polymer stabilization and CQ entrapment in hydrophobic domains of MD-3 (CQ / PSS = 0.1, 200 PSS monomers and 20 CQ at 300 K) (A) and MD-4 (CQ / PSS = 0.4, 200 PSS monomers and 80 CQ at 300 K) (B). Color representations of PSS (gray) and CQ (yellow).

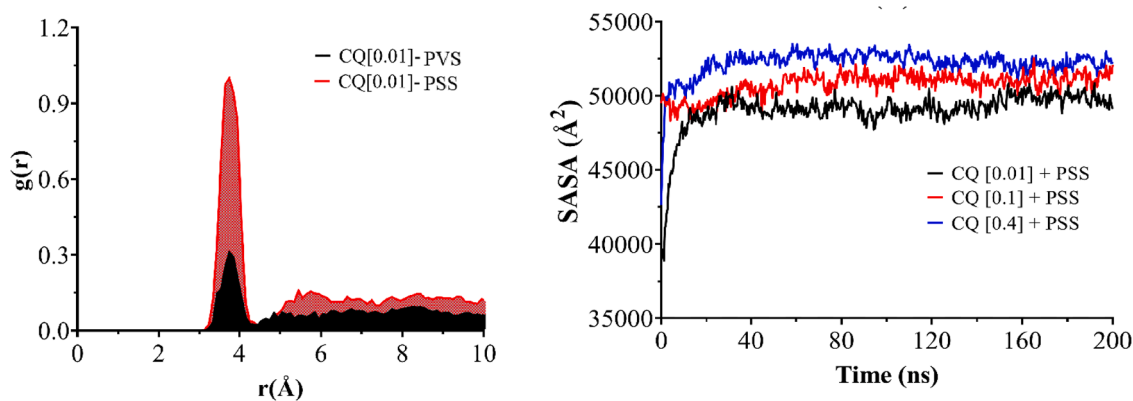


Fig. 4. Representative radial distribution functions ($g(r)$) between the quinoline nitrogen atom and the sulphur atom for PSS and PVS polymers (A). Solvent accessible surface area (SASA) for the PSS polymer at different CQ concentrations at 300 K (B).

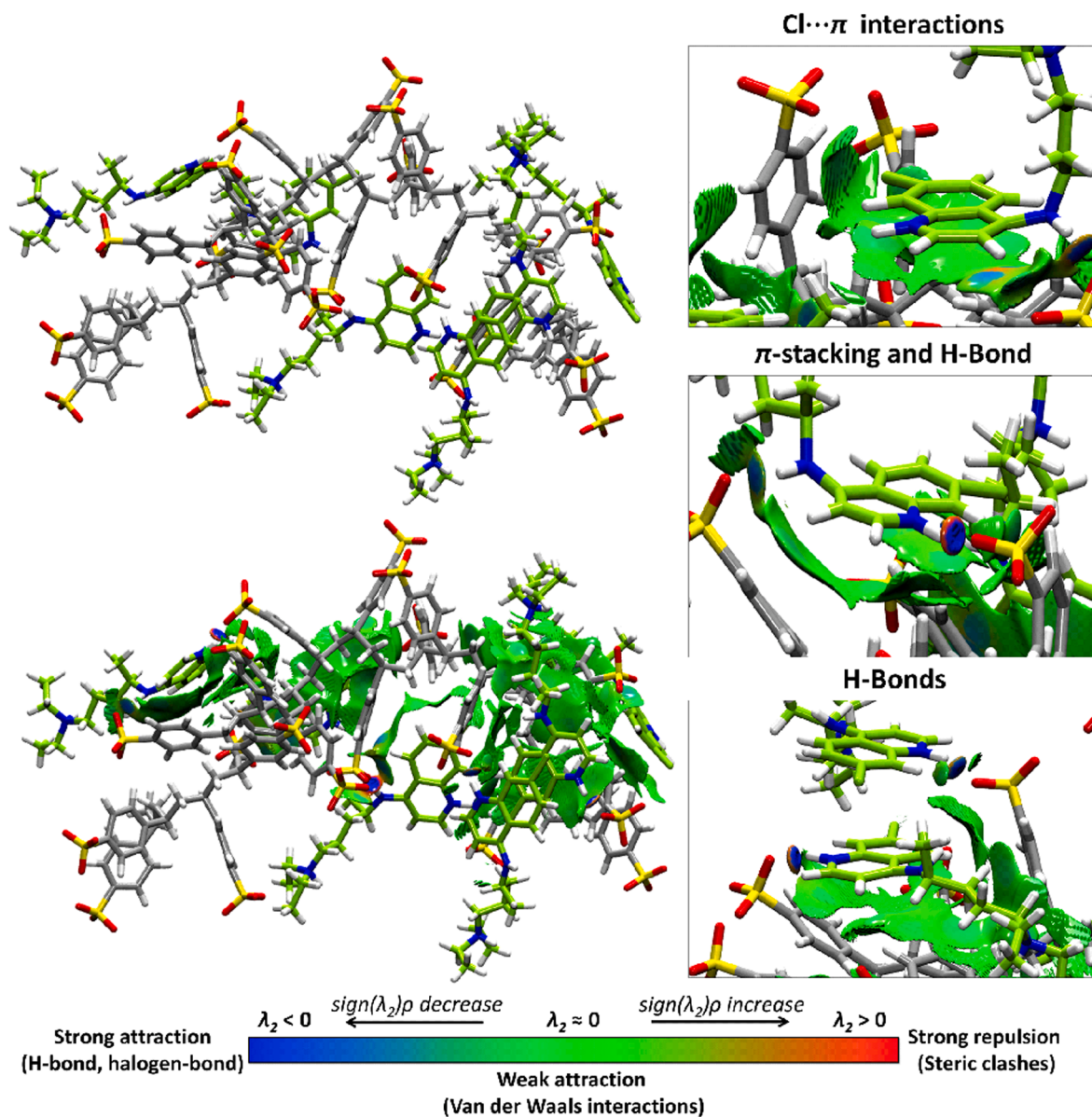


Fig. 5. Representative non-covalent interactions over the MD simulations for MD-1 (CQ / PVS = 0.01, 200 PVS monomers and 2 CQ at 300 K) (A) and MD-2 (CQ / PSS = 0.01, 200 PSS monomers and 2 CQ at 300 K) (B). The blue surfaces indicate strong attractive interactions, green indicates weak interactions, and red indicates overlap interactions. These calculations were performed at the promolecular electron densities.

are hydrogen bonding interactions of the quinoline nitrogen and tertiary amino group of CQ with the oxygens of the sulfonate group of PSS, in addition to aromatic π -stacking and Cl $\cdots\pi$ type interactions, where the aromatic π -stacking interactions are held between the aromatic quinoline group of CQ and the styrene group of PSS, and the halogen- π interactions are held between the chlorine of the aromatic quinoline group of CQ with the aromatic ring of the styrene of PSS.

To complement the all-atoms molecular simulation studies, coarse-grained MD simulations were performed to study the self-assembly of the PSS polymer encapsulating the CQ molecules in aqueous solution. Simulations for 6.5 μ s revealed that four PSS polymer chains, each composed of 80 NaSS monomers, are able to form a nanoparticle of approximately 10 nm in diameter (Fig. 6A), which is embedded in CQ molecules. This PSS nanoparticle is formed by the interaction of CQ molecules with each polymer chain, and hydrophobic self-assembly of the four resulting complexes, which in tandem encapsulates the CQ molecules, forming a uniform layer of CQ aggregates around the PSS polymer nanoparticle. Thus, the process of self-assembly and aggregate formation is divided into three steps (Fig. 6B) during the course of the molecular simulation (6.5 μ s in total): first, PSS chains interact with the CQ molecules; then, single chain CQ / PSS complex chains self-assemble forming aggregates; finally, a spherical, defined nanoparticle structure is formed, consisting of the four aggregated CQ / PSS complex chains; throughout the simulation, after the formation of the spherical PSS polymer nanoparticle the radius of gyration (R_{Gyr}) stabilizes until equilibrium is reached achieving a value of around 3 nm, indicating that the polymer is stabilized together with CQ molecules in the form of NPs, as can be seen in Fig. S3. This spherical structure of the PSS polymer is commonly accepted and proposed in the literature [63] showing an

interface between hydrophobic and hydrophilic regions. The extent of the hydrophobic regions increases with the increase of the number of ion pairs formed between the benzenesulfonate moieties and CQ molecules, thus enhancing the encapsulation of CQ molecules. The main driving force for the association is the hydrophobic interactions between the polymer backbone and the ion pairs resulting from the interaction of both CQ and PSS benzenesulfonate groups. It is important to note that these analyses are considering short polymer chains, highly diluted reactants, and short reaction times comparing with those that will be tested in bulk, thus, reasonably, larger NPs could be experimentally obtained.

3.2. CQ / PSS HLDNPs formation and characterization

The formation of CQ / PSS HLDNPs was experimentally evaluated. Conditions for HLDNPs formation were found at a fixed final polymer concentration of 3.3×10^{-3} M. Formulations with CQ / PSS molar ratio between 0.1 and 1.2 were developed. It is possible to observe in Fig. 6C that at low ratio (CQ / PSS = 0.1) clear solutions were obtained which are attributed to the presence of soluble complexes and/or low concentrated NPs. From CQ / PSS = 0.2 to 0.5, NPs suspensions were obtained, revealed by a notorious Tindall effect at naked eye. At CQ / PSS higher than 0.5 ratio, lower turbidity and the presence of macro-precipitates were evidenced, so that the colloidal state of the suspension collapses due to a higher PSS charge neutralization by the CQ counterions. As can be seen in Fig. 6D, NPs of hydrodynamic diameter in the range of 170 – 410 nm with PDI in the range of 0.25 – 0.47, are formed in the range CQ / PSS = 0.2 to 0.5, as seen by DLS. The corresponding zeta potential ranged between –18 and –45 mV, ensuring stability of the

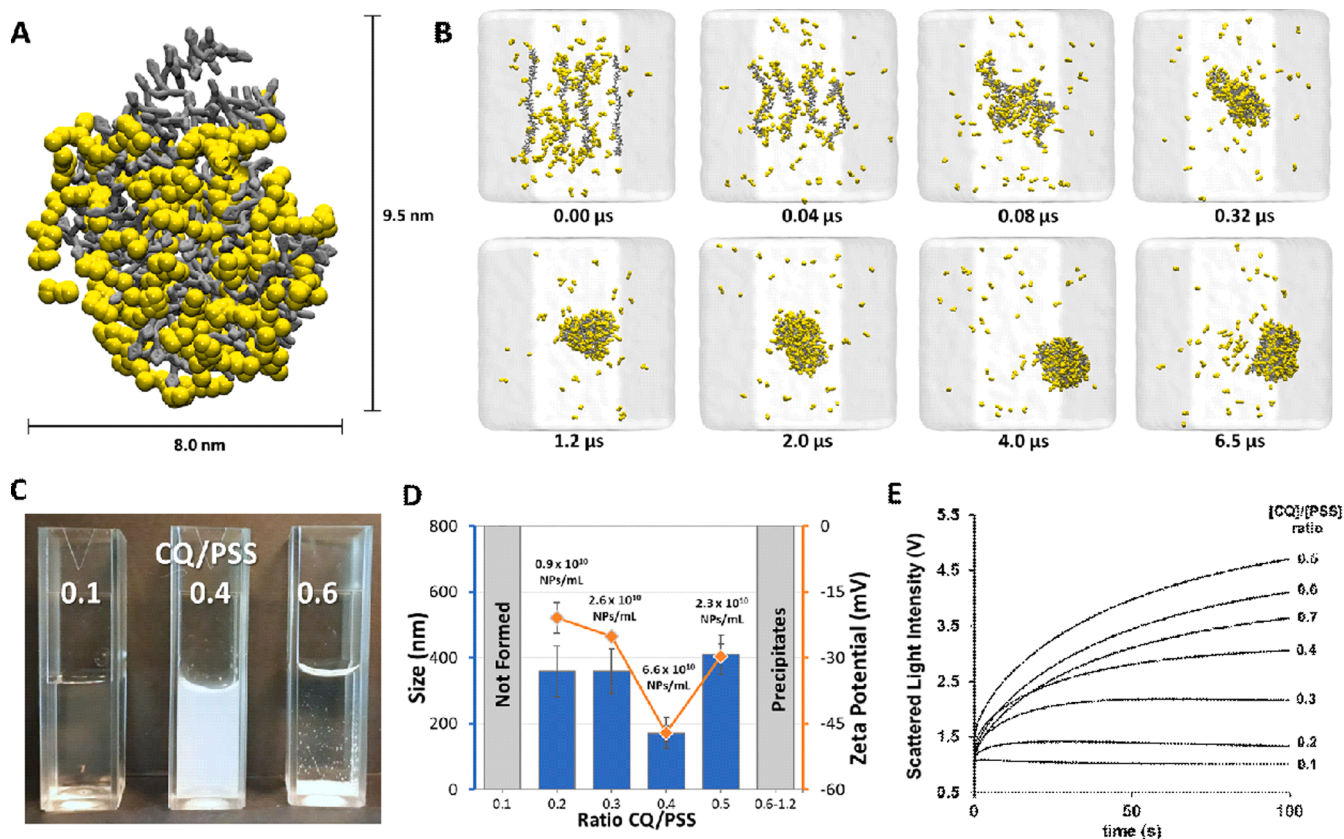


Fig. 6. Coarse-grained representation of the size of PSS polymer nanoparticle interacting with CQ molecules in simulations (last frame equivalent to 6.5 μ s). Color representations of PSS polymer (yellow) and CQ (gray) (A). Coarse-grained MD simulation showing the spontaneous formation of PSS polymer nanoparticle (on a time scale of 1.2 μ s) interacting with CQ molecules. Color representations of PSS (yellow) and CQ (gray) (B). Optical images of CQ / PSS 0.1, 0.4, 0.6 (C); Size (bars), zeta potential (rhombuses), and NPs concentration (number) of tested CQ / PSS formulations (mean \pm SD; n = 3) (D); Time dependence of scattered light after rapid mixing of PSS and CQ solutions (E).

NPs. Moreover, NTA evidenced nanoparticle concentrations in the range of 0.9×10^{10} to 6.6×10^{10} NPs / mL. The time dependence of scattered light intensity after mixing equal amounts of PSS and CQ solution at different CQ / PSS molar ratios was obtained using a stopped-flow reactor, and the results are shown in Fig. 6E. This process was monitored for 100 s. We observed that for low CQ / PSS molar ratio (i.e., 0.1 and 0.2) the scattered light was weak, consistent with the absence or the presence of a very few number of particles, as shown by DLS and NTA. The data for CQ / PSS compositions in the range of 0.3 to 0.7 were fitted using two non-linear functions corresponding to a monoexponential (Equation (3)) and a biexponential function (Equation (4)), respectively (see Tables S3 and S4). For monoexponential fitting we observed that fitted data did not match with the scattered data at low times. However, the fitting is improved by using a biexponential function. In this case, χ^2 obtained for the biexponential fitting is one order of magnitude lower than the obtained for the monoexponential fitting [67]. Similar results have been observed during the formation of supramolecular structures such as complementary charged polyelectrolyte complexes [79], pH induced micellization [80], and in the formation of polyion micelles complexes of positive and negative block copolymers such as PSS-*b*-PEO [81]. These results indicate that NPs formation after rapid mixing is dominated by two continuous processes occurring with different rate. The first fast process, where scattered light increases with a large amplitude (C1 parameter in Table S4), is associated to the formation of continuous polymer-drug assemblies in a quasi-equilibrium state formation; the latter slow processes, where scattered light increases with a low amplitude (C2 parameter, Table S4), is related to the formation of final equilibrium CQ / PSS complexes from previously formed aggregates in the rapid process [67,82]. This mechanism is consistent with the coarse-grained simulations seen in Fig. 6A-B, although the time scale is much longer. It is interesting to note that the scattered light intensity at longer times increases up to a CQ / PSS = 0.5, and then decreases, possibly due to the formation of polydisperse suspensions, consistent with the results shown by DLS and microprecipitation seen at naked eye.

The results obtained at CQ / PSS = 0.4 are outstanding: this formulation shows the smallest HLDNPs with the lowest size Pdl (0.25), and with the lowest zeta potential (higher stability), and at the same time the highest NP concentration. STEM images of this formulation show uniform spheroidal structures (Fig. 7A) whose size is smaller than that shown by DLS. These results could reflect the hydrated and partially swollen state of the HLDNPs in water that shrink in the drying process during sample preparation for STEM. In the case of CQ / PVS formulations explored as control, NPs are also found in the same composition range, which disappears upon addition of NaCl (100 and 200 mM) (Fig. 7B), suggesting weaker interactions between the two components, mainly attributed to electrostatic interactions between the oppositely charged molecules, allowing the formation of NPs by ionic self-assembly. As said above, the observed behaviour typically occurs when electrostatic forces are dominant on the overall interactions since these interactions are cleaved by the ionic strength. Thus, CQ / PVS NPs

(CQ / PVS = 0.4) show size of ≈ 70 nm, Pdl of ≈ 0.2 , and zeta potential of ≈ -20 mV in the absence of NaCl, and the interaction is cleaved in the presence of the added electrolyte. On the contrary, the selected CQ / PSS NPs (CQ / PSS = 0.4) are stable in terms of size and zeta potential under increasing NaCl concentrations with minimal deviations. This is an important fact, since NaCl is ubiquitously present in the body fluids [8,83,84]; thus, these results aim at ensuring stability of the CQ / PSS formulations into the body.

Due to the outstanding stability of these CQ / PSS NPs (CQ / PSS = 0.4) in the presence of aqueous NaCl, further studies have been done to provide important pharmaceutical and industrial information. Thus, the stability of the obtained NPs at CQ / PSS = 0.4 was also studied under other biological and challenging storage conditions. As can be seen in Fig. S4, results show that the CQ / PSS HLDNPs (CQ / PSS = 0.4) are widely stable under temperature variations, pH gradient, and prolonged storage, with minimal deviations. For this formulation (CQ / PSS = 0.4) we also analysed two very important technological parameters: *AE*, which achieved 99.8 %, and *DL*, which took values as high as 48.6 %. The achieved values indicate that only a negligible mass of drug is not interacting with the selected polymer (0.2 %), and that the interacting molecules of CQ represent half of the mass in each NP. These results are impressive and highlight the strategy of providing aromatic-aromatic drug-polymer interactions as a complement to obtain nanoformulations based on ionic assembling.

The release profiles of the HLDNPs CQ / PSS 0.4 were obtained by conventional dialysis and continuous dissolution (USP 4 dissolution apparatus) both in water and in simulated body fluid. A sustained and prolonged release of CQ from the HLDNPs in Milli-Q water was evidenced. The cumulative CQ release by dialysis, as a function of time, showed a maximum of 3 % in 30 days (Fig. 8A-a). In this experiment, the binding between the aromatic CQ and the aromatic polymer PSS remains mostly unaltered, and the release is conditioned by the fraction of CQ molecules located on the surface of the NPs (thermodynamically bound) and thus available to be released. Under simulated biological conditions (0.13 M NaCl, pH 7.4, and 37 °C) a biphasic release of CQ from HLDNPs CQ / PSS 0.4 was evidenced with an initial release phase (≈ 50 % in 24 h), followed by a controlled and prolonged release until 30 days (Fig. 8A-b). This controlled and prolonged release profile represents a large improvement over other nanoformulations encapsulating CQ. Indeed, release of 81 % of CQ was obtained during the first hour for the CQ / PVS NPs (CQ / PVS = 0.4) in simulated biological conditions (data not shown). Moreover, with the aim of studying a more dynamic process, the continuous flow cell apparatus USP 4 was used (Fig. 8A-c). As could be expected, a larger cumulative release of 16.2 % in the first 6 h was found, demonstrating that the exposition of these NPs to a continuous flux of medium accelerates the release of CQ. Furthermore, the release mechanism obtained by the fit of the data to different models (i.e., zero order, first order, Higuchi and Korsmeyer-Peppas) was assessed. The Korsmeyer-Peppas fitted better to the data (Fig. 8B). Considering the features of the components (hydrophilic molecules),

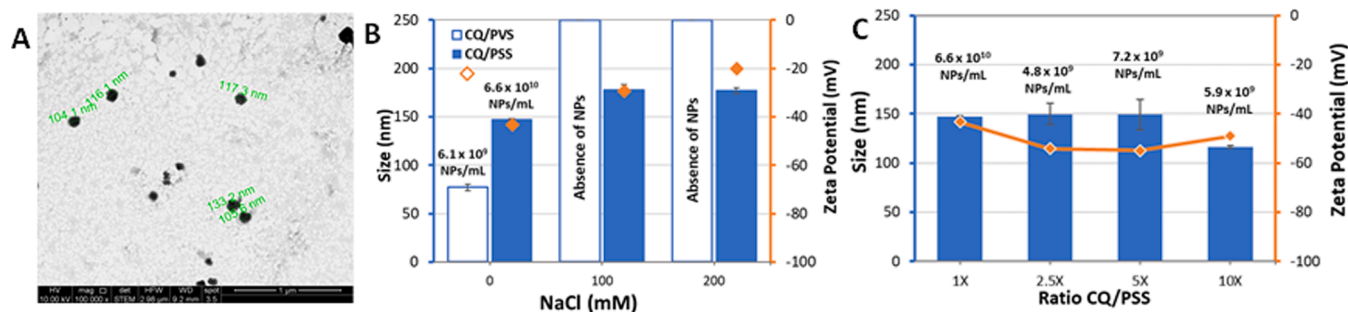


Fig. 7. STEM image of NPs CQ / PSS 0.4 (A); Ionic strength stability of CQ / PSS 0.4 and CQ / PVS 0.4 NPs through evaluation of size (bars) and zeta potential (rhombuses) as a function of different NaCl concentrations (mean \pm SD, n = 3) (B); Size (bars), zeta potential (rhombuses), and NPs concentration (number) for CQ / PSS 0.4 scaling up (mean \pm SD; n = 3) (C).

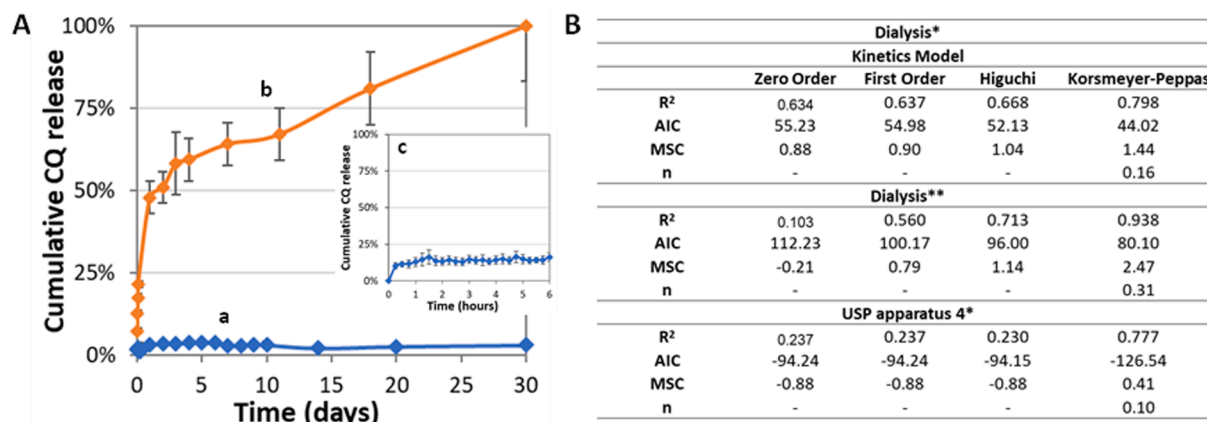


Fig. 8. Cumulative CQ release (%) of CQ/PSS 0.4 NPs evaluated by conventional dialysis (A) in Milli-Q water (a) and simulated biological medium (b), and by continuous flow cell USP 4 apparatus in Milli-Q water (c) (mean \pm SD, n = 3) (A). Values of CQ release data obtained from kinetic models for conventional dialysis and USP 4 apparatus at different conditions (Milli-Q water* and simulated biological conditions**) (B).

and that CQ is a structural component of the NPs, the drug release should involve the release of CQ from the surface of the NPs, due to equilibrium displacement, and followed by hydration and rearrangement of the boundary between the inner and the surface of the NPs. The detachment of CQ from the NPs enhances the hydration of the system, so that the subjacent confined drug molecules achieve a hydrated environment and a new equilibrium state with the bulk is established. This process progresses in a cyclic manner. This complex process is consistent with deviations of the linear or first order behaviour of the release as a function of time, thus being consistent with the Korsmeyer-Peppas model.

3.3. Final remarks and perspectives

This simple strategy of encapsulation of CQ, producing the outstanding characteristics of the HLDNPs CQ / PSS 0.4 in terms of green synthesis, using only water as solvent, high values of AE and DL, and good stability, responsible for a controlled release of the drug in days, can be compared with other strategies reported in the literature (see Table 1). An encapsulation strategy that also avoids the use of organic solvents is the use of Pluronic® as excipient to form polymeric NPs micelles, able to encapsulate with 72 % of efficiency. An interesting approach of encapsulation of CQ with only one excipient consisted of the formation of CQ / polymer soluble salts with poly(amidoamine)s polymers, but involved the transformation of the drug in its free base and addition in alcoholic medium. These systems showed, however, fast release during 24 h. With the use of acetone, dextran NPs could be synthesized containing CQ, showing DL of 40 %, AE of 81 %, and 90 % release in 8 h. Reports were found encapsulating CQ in chitosan/tripolyphosphate NPs obtained by ionic gelation. However, the associated pharmaceutical performance, when reported, was not optimal, as can be seen in Table 1. Ionic gelation has the advantage of being produced in water, similar to our encapsulation strategy. Poly(ethylene glycol) (PEG)-iron NPs able to encapsulate CQ were also synthesized in water, showing DL of 28 %, and AE of 99 %. Gelatin-glutaraldehyde NPs have also been synthesized in emulsion using organic solvents. The resulting particles were able to swell in water releasing the drug in 2 h. Other strategies consist of the encapsulation of the drug in water-insoluble solid NPs, obtained by different methods, all of them using an organic solvent for their production. Thus, NPs made with biodegradable polyesters such as poly(lactide) (PLA) or poly(lactic-co-glycolic) acid (PLGA) were used to successfully encapsulate CQ, with high AE, but moderate DL. Formation of micelles of these polyesters with the aid of hydrophilic polymers such as polysaccharides and PEG to afford smaller particles easily dispersible in water have also been reported. Solid lipid nanoparticles have been also assayed to encapsulate CQ, some of which do also show surface modification with hydrophilic components.

Table 1

Results of encapsulation of CQ with different strategies.

Encapsulation system	Release / time	DL (%)	AE (%)	Reference
PSS NPs	65 % / 10 days	48.6	99.8	This work
Pluronic F-127 micelles	-	-	72	[99]
Poly(amidoamine)s polymers water soluble salts	70—80 % / 24 h	14—33	-	[100101]
Dextran NPs	90 % / 8 h	40	81	[102]
Chitosan-tripolyphosphate nanogels	-	27	54	[103104105106]
Chitosan- <i>Sterculia striata</i> polysaccharides nanogels	40 – 60 % / 24 h	-	28	[107]
Dehydroascorbate-derivatized chitosan tripolyphosphate nanogels	80 % / 72 h	40	50 – 57	[108]
PEG-iron NPs	-	28	99	[109]
Gelatin-glutaraldehyde NPs	90 % / 2 h	17—19	-	[110]
PLA NPs	40 % / 6 h	-	64	[111]
PVA-PLA NPs	-	-	-	[99]
PLGA NPs	70 % / 24 h (pH 5) 20 % / 24 h (pH 7)	12.92	76.2	[112]
PEG-PLGA micelles	-	7.1	72.8	[113]
Polysaccharide-PLGA micelles	20 – 80 % / 24 h	11	88	[114]
Solid lipid NPs	-	-	93.5	[115]
Heparin surface-modified solid lipid NPs	60 – 80 % / 2 h	21 – 25	78—90	[116]

The outstanding high stability of HLDNPs such as CQ / PSS 0.4 is pivotal to provide prolonged release in selected tissues/sites of administration, potentially improving the therapeutic response of the drug during long treatments. For instance, projecting a prolonged drug delivery after intramuscular administration represents a plausible possibility. Although it can be assumed high stability and prolonged release using this administration site, providing a pharmacokinetic profile similar to the release behaviour presented in this paper, factors other than physiological pH and ionic strength of this tissue, such as the presence of enzymes, specific ions, flux of components, vasculature, etc. will also contribute to determine a final pharmacokinetic profile. In

addition, the pharmacodynamic response can be also affected by the presence of soluble chains of PSS by competing with the target receptor.

The development of a medicine with controlled release of CQ could be an option to prevent its important side effects such as retinopathy, cardiomyopathy, myopathy, and neuromyopathy, enhancing its potential for a variety of illness where CQ has been tested or is under investigation (rheumatoid arthritis, systemic lupus erythematosus, spondylitis, rosacea, cancer, diabetes, atherosclerosis, dermatomyositis, and Sjögren's syndrome) [18]. It is worth to mention that, for the COVID-19 pandemic, CQ was initially proposed to prevent the contagion, but the occurrence of adverse side effects was a big argument against the use of the drug [85]. In order to project industrial elaboration for the CQ / PSS 0.4 formulation, up-scaling for 2.5, 5, and 10X have been tested. As seen in Fig. 7C, all tested formulations allowed obtaining monodisperse and negatively charged HLDNPs. Interestingly, a slight tendency to obtain smaller size and less concentrated NPs is evidenced, which could be faced with proper engineering solutions when required at the industry scale [86–88]. The selected elaboration strategy, compared with other conventional methods, provides several advantages for scalability, such as avoiding organic solvents, allowing low energy consumption, feasibility at room temperature, or suppression of solvent evaporation steps. In addition, the high stability of the formulations also influences the quality of the product if the final formulation is not transformed to powder, since the liquid form can be safely transported and stored, or, if converted into powder, the further reconstituted formulation can be preserved for multiple administrations. Nevertheless, stirring to form vortex or turbulence at large scale during the mixture, or, if needed, using freeze-drying at large scale could represent challenges to be faced in large scale production. Although PSS is approved by the FDA, showing several therapeutic potential uses [89], toxicity is associated to its prolonged use, producing hypomagnesemia, hypocalcemia, colonic necrosis, and sodium load, potentially precipitating worsening hypertension and congestive heart failure symptoms [90]. Thus, although the presented strategy to create nanoparticles has high potential, further experimentation to project real medicines is required. Final formulations must be tested in *in vitro* and *in vivo* models to identify safety and efficacy.

As described previously, the occurrence of aromatic-aromatic interactions with aromatic polymers in our formulations is critical for their high performance, allowing the significantly prolonged drug release for HLDNPs CQ / PSS 0.4, and its improved stability even in the presence of salt and under different pH values. The role of aromatic-aromatic interactions has been highlighted by theoretical calculations. Quantum mechanics calculations pointed at a higher binding energy between CQ and PSS due to π -stacking interactions, ranging from -17.81 to -26.89 kcal/mol, in contrast with CQ and PVS with binding energies ranging from -7.87 to -6.32 kcal/mol. This significant difference indicates a stronger binding affinity for CQ / PSS [91]. Indeed, PSS contains an aromatic styrene group that facilitates π -stacking and hydrophobic interactions with the aromatic quinoline ring of CQ. These aromatic-aromatic interactions contribute with additional binding energy beyond electrostatic interactions, unlike PVS, which lacks an aromatic group and interact mainly electrostatically. This indicates that π -stacking provides stronger binding between the polymer and the drug that drives the self-assembly into stable NPs, as further seen by MD simulations. MD simulations demonstrated that CQ aggregates around PSS chains, while remains free in solution with PVS. This observation underscores the favourable hydrophobic interactions between CQ and the aromatic rings of PSS. MD simulations served, then, as a pivotal tool in unravelling the intricacies of the aggregation and formation processes inherent in HLDNPs containing CQ and PSS. In the complex interplay of molecular forces, key findings emerged, shedding light on the dynamic interactions at play. Zooming into the microscopic realm, all-atom MD simulations uncovered the aggregation of CQ around PSS chains, forming a robust interface that catalyzes nanoparticle formation. The driving forces behind this phenomenon are identified as hydrophobic

interactions and the prevalent π -stacking interactions between CQ and PSS. Further exploration through coarse-grained MD simulations unveiled the spontaneous formation of NPs. Good match with the experimental results were found. Experimental validation came in the form of mixing CQ and PSS solutions. NMR studies revealed that the aromatic protons of CQ are strongly influenced by PSS, indicating close contacts caused by aromatic-aromatic interactions. Conversely, no such effect is observed with the non-aromatic PVS. The additional binding energy in the CQ / PSS system enables the NPs to remain stable even in high-salt conditions, unlike the CQ / PVS NPs, which disassemble. This further supports the hydrophobic stabilization of CQ / PSS, highlighting the superiority of hydrophobic and π -stacking interactions over purely electrostatic forces, leading to rapid NP formation within seconds to minutes, as evidenced by stopped-flow measurements. The experimental kinetic analysis fitted with a biexponential model, pointing at a two-step mechanism involving aggregate formation and subsequent reorganization, as arising from the theoretical calculations. Discrepancies in size are rationalized by considering factors such as higher polymer molecular weight, higher concentration, and extended assembly times in the experimental setup. In contrast, weak interactions and unstable formulations are seen with the aliphatic polymer, both theoretically and experimentally, indicating that aromatic-aromatic interactions were critical for the high stability and high loading. Aromatic-aromatic interactions impart stability and high loading capacity not achievable with non-aromatic components [92,93].

The stability of HLDNPs is intricately governed by a network of non-covalent interactions, each playing a vital role in shaping the characteristics of these advanced drug delivery systems. Hydrophobic interactions emerge as key orchestrators in the self-assembly of HLDNPs, particularly in the presence of hydrophobic drugs and polymers. This phenomenon not only facilitates self-assembly but also amplifies the drug loading capacity, creating a robust foundation for the nanoparticle structure. Electrostatic interactions further contribute to stability, manifesting as hydrogen bonding or ionic interactions between charged or polar groups on drugs and polymers. This dynamic interplay not only enables high drug loading but also serves as a barrier against premature release, ensuring that the therapeutic payload reaches its intended destination with precision. The inclusion of van der Waals forces and π -stacking adds an additional layer of stability to the loaded nanoparticles. These forces act as binding agents, fortifying the structure and preventing unintended disassembly. The synergy among these non-covalent interactions, even accounting for individually weak forces like London dispersion, cumulatively reinforces the stability of HLDNPs. Crucially, these interactions act as molecular locks, immobilizing drug molecules within the polymer matrix. This confinement effectively curtails the potential for crystallization or phase separation, thereby upholding the colloidal stability of the nanoparticles over time. Comparatively, non-covalent loading proves superior in preserving the activity of drug molecules when contrasted with covalent linkage. This strategy not only safeguards the bioactivity of the encapsulated drugs but also facilitates efficient intracellular release, enhancing the therapeutic efficacy of the HLDNP delivery system. Due to the complexity of the spontaneous forces involving aromatic drugs / polyelectrolytes interactions (of aromatic and non-aromatic nature) in aqueous medium, the combination of strategies to understand and project specific responses is ideal. In this paper, several quantum chemical calculations and MD tools were applied in combination with experimental analyses. In essence, the computational simulations not only unravel the atomic-level intricacies of CQ / PSS interactions, aggregation, and nanoparticle assembly mechanisms but also closely mirror experimental observations. These simulations emerge as a potent tool, offering valuable insights for the rational design and optimization of HLDNP formulations, bridging the gap between theory and experimentation in the realm of nanomedicine [94–98]. To achieve a good match between theoretical and experimental results, it is necessary to provide a good characterization of the molecules, with pivotal features such as total charge, and

an appropriate strategy to include the solvent effects. The contrasted results (theoretical and experimental) could help us for a better understanding of the whole phenomena, and their application and refinement would promote the general efficient design and production of drug / polyelectrolyte formulations with therapeutical potential.

4. Conclusions

In conclusion, our investigation offers selected theoretical and experimental tools that allow the exploitation of aromatic interactions to provide very efficiently synthesized HLDNPs. The strategy involves taking advantage of site-specific short-range interactions (hydrogen bond, π -stacking, and van der Waals), between one dicationic and aromatic drug, such as CQ, and one anionic and aromatic polymer, such as PSS (as unique excipient), for the stabilization of ionically interacting components, as deduced by UV-vis, ^1H NMR, and quantum mechanics and molecular dynamics. Due to these secondary short-range interactions, ion pairs are formed and further stabilized in hydrophobic polymer domains, showing binding energies of $-17 - -27$ kcal/mol, significantly higher in absolute value than those found for the system CQ / PVS ($-6 - -8$ kcal/mol). MD simulations, after combining short polymer chains, highly diluted reactants and short reaction times, revealed that PSS forms a nanoparticle of 10 nm in diameter embedded in CQ molecules. This process is preceded by the aggregation of CQ around the PSS polymer chains, forming an interface between components, and thus, enhancing aggregation. Experimentally obtained HLDNPs showed low polydispersity ($\text{PdI} = 0.25 - 0.47$), diameter of 170 – 410 nm, and negative zeta potential ($-18 - -45$ mV). We demonstrated that the strategy for elaboration, after simply mixing two aqueous liquids, can be scaled up, with minimal deviations in size, PDI, zeta potential, and number of formed NPs. Values of association efficiency and drug loading were very high (99.8 % and 48.6 %, respectively) and the formulations were stable to NaCl exposure, pH gradient, temperature, and long-term storage; in addition to provide prolonged drug release (until 30 days). Due to the complexity of the spontaneous forces involving aromatic drug / aromatic polyelectrolyte interactions in aqueous medium, the combination of the proposed theoretical and experimental tools could be strategical for the design, development, analysis and scale up for particular drug / polymer combinations to provide nanomedicines.

This work was supported by FONDECYT 3210549 (M.G.V-S), FONDECYT 1201899 (F.A.O-A.), FONDECYT 1210968 (I.M-V.), FONDEQUIP EQM160157 (F.A. O-A), FONDEQUIP EQM150106 (J.G.), ANID/PIA/ACT192144 (F.A. O-A) FONDAP 15130011 (F.A. O-A) and ANID PhD fellowship award 21,202,337 (G.A-A).

Authors contributions

M.G.V-S developed the experimental section and contributed with the writing of the manuscript. O.Y developed the theoretical section and contributed with the writing of the manuscript. M.E.F contributed with the performance and analysis of the stopped-flow experiments. G.A.A contributed with the scaling-up formulations. J.G. contributed with the NMR experiments. F.G.-N guided all the theoretical section and contributed with the writing of the manuscript. I.M-V and F.A.O-A guided all the experimental section and contributed with the writing of the manuscript.

CRedit authorship contribution statement

María Gabriela Villamizar-Sarmiento: . **Osvaldo Yáñez:** . **Mario E. Flores:** Investigation, Methodology. **Gonzalo Álvarez-Acevedo:** . **Fernando González-Nilo:** Conceptualization. **Juan Guerrero:** . **Ignacio Moreno-Villoslada:** Conceptualization, Funding acquisition, Project administration, Resources, Supervision, Validation, Writing – original draft, Writing – review & editing. **Felipe A. Oyarzun-Ampuero:** Conceptualization, Funding acquisition, Project administration, Resources, Supervision, Validation, Writing – original draft, Writing – review & editing.

Declaration of competing interest

The authors declare that they have no known competing financial interests or personal relationships that could have appeared to influence the work reported in this paper.

Data availability

Data will be made available on request.

Appendix A. Supplementary data

Supplementary data to this article can be found online at <https://doi.org/10.1016/j.molliq.2023.123906>.

References

- [1] B. Begines, et al., Polymeric Nanoparticles for Drug Delivery: Recent Developments and Future Prospects, *Nanomaterials* 10 (2020), <https://doi.org/10.3390/nano10071403>.
- [2] K.M. El-Say, H.S. El-Sawy, Polymeric nanoparticles: Promising platform for drug delivery, *Int. J. Pharm.* 528 (1) (2017) 675–691.
- [3] A. Sánchez, S.P. Mejía, J., Orozco Recent Advances in Polymeric Nanoparticle-Encapsulated Drugs against Intracellular Infections, *Molecules* 25 (2020), <https://doi.org/10.3390/molecules25163760>.
- [4] A. Zielińska, et al., Polymeric Nanoparticles: Production, Characterization, Toxicology and Ecotoxicology, *Molecules* 25 (2020), <https://doi.org/10.3390/molecules25163731>.
- [5] E. Lallana, et al., Click Chemistry for Drug Delivery Nanosystems, *Pharm. Res.* 29 (1) (2012) 1–34.
- [6] B. Lu, A. Atala, Chapter 6 - Small Molecules: Controlling Cell Fate and Function, in: S.J. Lee, J.J. Yoo, A. Atala (Eds.), *In Situ Tissue Regeneration*, Academic Press, Boston, 2016, pp. 87–110.
- [7] V. Tomar, et al., Small Molecule Drug Design, in: S. Ranganathan (Ed.), *Encyclopedia of Bioinformatics and Computational Biology*, Academic Press, Oxford, 2019, pp. 741–760.
- [8] M.G. Villamizar-Sarmiento, et al., A New Methodology to Create Polymeric Nanocarriers Containing Hydrophilic Low Molecular-Weight Drugs: A Green Strategy Providing a Very High Drug Loading, *Mol. Pharm.* 16 (7) (2019) 2892–2901.
- [9] O.P. Varghese, et al., Chondroitin sulfate derived theranostic nanoparticles for targeted drug delivery, *Biomater. Sci.* 4 (9) (2016) 1310–1313.
- [10] X. Jin, et al., Supramolecular nanoscale drug-delivery system with ordered structure, *Natl. Sci. Rev.* 6 (6) (2019) 1128–1137.
- [11] M.G. Villamizar-Sarmiento, et al., The key role of the drug self-aggregation ability to obtain optimal nanocarriers based on aromatic-aromatic drug-polymer interactions, *Eur. J. Pharm. Biopharm.* 166 (2021) 19–29.
- [12] W.L. Jorgensen, D.L. Severance, Aromatic-aromatic interactions: free energy profiles for the benzene dimer in water, chloroform, and liquid benzene, *J. Am. Chem. Soc.* 112 (12) (1990) 4768–4774.
- [13] Hunter, C.A., et al., Aromatic interactions. *Journal of the Chemical Society, Perkin Transactions 2*, 2001(5): p. 651–669.
- [14] E.A. Meyer, R.K. Castellano, F. Diederich, Interactions with Aromatic Rings in Chemical and Biological Recognition, *Angew. Chem. Int. Ed.* 42 (11) (2003) 1210–1250.
- [15] M.D. Conrad, P.J. Rosenthal, Antimalarial drug resistance in Africa: the calm before the storm? *Lancet Infect. Dis.* 19 (10) (2019) e338–e351.
- [16] P. Schlagenhauf, et al., 15 - Malaria Chemoprophylaxis, in: J.S. Keystone (Ed.), *Travel Medicine* (fourth Edition), Elsevier, London, 2019, pp. 145–167.
- [17] E. Schrezenmeier, T. Dörner, Mechanisms of action of hydroxychloroquine and chloroquine: implications for rheumatology, *Nat. Rev. Rheumatol.* 16 (3) (2020) 155–166.
- [18] F. Antonis, K.B. George, T.B. Dimitrios, Chloroquine as alternative antimalarial in systemic lupus erythematosus. Response to ‘2019 update of the EULAR recommendations for the management of SLE: don’t forget chloroquine’ by Figueroa-Parra et al, *Ann. Rheum. Dis.* 79 (9) (2020) e115.
- [19] Lupus Foundation of America. Why are treatments that were developed for malaria now used for lupus? 2020.
- [20] Y. Zhang, et al., Chloroquine (CQ) exerts anti-breast cancer through modulating microenvironment and inducing apoptosis, *Int. Immunopharmacol.* 42 (2017) 100–107.
- [21] M.P. Hage, M.R. Al-Badri, S.T. Azar, A favorable effect of hydroxychloroquine on glucose and lipid metabolism beyond its anti-inflammatory role, *Ther. Adv. Endocrinol. Metab.* 5 (4) (2014) 77–85.
- [22] R.F. de Almeida Júnior, et al., Chloroquine as a promising adjuvant therapy for type 1 Diabetes Mellitus, *Sci. Rep.* 10 (1) (2020) 12098.
- [23] A.M. Shukla, et al., Impact of Hydroxychloroquine on Atherosclerosis and Vascular Stiffness in the Presence of Chronic Kidney Disease, *PLoS One* 10 (9) (2015) e0139226.

- [24] C.O. Anyanwu, et al., The systemic management of cutaneous dermatomyositis: Results of a stepwise strategy, *International Journal of Women's Dermatology* 3 (4) (2017) 189–194.
- [25] H.J. Lee, et al., The Effect of Chloroquine on the Development of Dry Eye in Sjögren Syndrome Animal Model, *Invest. Ophthalmol. Vis. Sci.* 60 (12) (2019) 3708–3716.
- [26] R.A. Boto, et al., NCIPLLOT4: Fast, Robust, and Quantitative Analysis of Noncovalent Interactions, *J. Chem. Theory Comput.* 16 (7) (2020) 4150–4158.
- [27] A. Otero-de-la-Roza, E.R. Johnson, J. Contreras-García, Revealing non-covalent interactions in solids: NCI plots revisited, *PCCP* 14 (35) (2012) 12165–12172.
- [28] J. Contreras-García, et al., NCIPLLOT: A Program for Plotting Noncovalent Interaction Regions, *J. Chem. Theory Comput.* 7 (3) (2011) 625–632.
- [29] E.R. Johnson, et al., Revealing Noncovalent Interactions, *J. Am. Chem. Soc.* 132 (18) (2010) 6498–6506.
- [30] C. Lefebvre, et al., Accurately extracting the signature of intermolecular interactions present in the NCI plot of the reduced density gradient versus electron density, *PCCP* 19 (27) (2017) 17928–17936.
- [31] J. Contreras-García, W. Yang, E.R. Johnson, Analysis of Hydrogen-Bond Interaction Potentials from the Electron Density: Integration of Noncovalent Interaction Regions, *Chem. A Eur. J.* 115 (45) (2011) 12983–12990.
- [32] T.V. Hunt, et al., Single-dose sodium polystyrene sulfonate for hyperkalemia in chronic kidney disease or end-stage renal disease, *Clin. Kidney J.* 12 (3) (2019) 408–413.
- [33] J.C. Hollander-Rodríguez, J.F. Calvert Jr., Hyperkalemia, *Am Fam Physician* 73 (2) (2006) 283–290.
- [34] S. Garg, et al., Development and Characterization of Bioadhesive Vaginal Films of Sodium Polystyrene Sulfonate (PSS), a Novel Contraceptive Antimicrobial Agent, *Pharm. Res.* 22 (4) (2005) 584–595.
- [35] A.S. Pranti, et al., PEDOT: PSS coating on gold microelectrodes with excellent stability and high charge injection capacity for chronic neural interfaces, *Sens. Actuators B* 275 (2018) 382–393.
- [36] A. Schander, et al., Design and fabrication of novel multi-channel floating neural probes for intracortical chronic recording, *Sens. Actuators, A* 247 (2016) 125–135.
- [37] P. Pattanauwat, M. Tagaya, T. Kobayashi, Controllable nanoporous fibril-like morphology by layer-by-layer self-assembled films of bioelectronics poly (pyrrole-co-formyl pyrrole)/polystyrene sulfonate for biocompatible electrode, *Mater. Res. Bull.* 99 (2018) 260–267.
- [38] O. Yañez, et al., (Li6Si5)2–5: The Smallest Cluster-Assembled Materials Based on Aromatic Si56–Rings. *Chemistry – A, European Journal* 25 (10) (2019) 2467–2471.
- [39] M.F. Manrique-de-la-Cuba, et al., Li8Si8, Li10Si9, and Li12Si10: Assemblies of Lithium-Silicon Aromatic Units, *ChemPhysChem* 22 (10) (2021) 906–910.
- [40] R. Báez-Grez, et al., Exploring the Potential Energy Surface of Trimetallic Deltahedral Zintl Ions: Lowest-Energy [Sn6Ge2Bi]3– and [(Sn6Ge2Bi)2]4– Structures, *Inorg. Chem.* 58 (15) (2019) 10057–10064.
- [41] P. Cantero-López, et al., Theoretical and experimental approach on the molecular interactions of the DL-Alanine with an electrolytic environment, *Chem. Phys. Lett.* 687 (2017) 73–84.
- [42] O. Yañez, et al., Kick-Fukui: A Fukui Function-Guided Method for Molecular Structure Prediction, *J. Chem. Inf. Model.* 61 (8) (2021) 3955–3963.
- [43] F. Avila-Salas, et al., Study of Interaction Energies between the PAMAM Dendrimer and Nonsteroidal Anti-Inflammatory Drug Using a Distributed Computational Strategy and Experimental Analysis by ESI-MS/MS, *J. Phys. Chem. B* 116 (7) (2012) 2031–2039.
- [44] P.P. Bera, et al., Mindless Chemistry, *Chem. A Eur. J.* 110 (13) (2006) 4287–4290.
- [45] M. Saunders, Stochastic exploration of molecular mechanics energy surfaces. Hunting for the global minimum, *J. Am. Chem. Soc.* 109 (10) (1987) 3150–3152.
- [46] M. Saunders, Stochastic search for isomers on a quantum mechanical surface, *J. Comput. Chem.* 25 (5) (2004) 621–626.
- [47] A.V. Sulimov, et al., Combined Docking with Classical Force Field and Quantum Chemical Semiempirical Method PM7, *Adv. Bioinforma.* 2017 (2017) 7167691.
- [48] J.J.P. Stewart, MOPAC: A semiempirical molecular orbital program, *J. Comput. Aided Mol. Des.* 4 (1) (1990) 1–103.
- [49] C. Adamo, V. Barone, Toward reliable density functional methods without adjustable parameters: The PBE0 model, *J. Chem. Phys.* 110 (13) (1999) 6158–6170.
- [50] S. Grimme, S. Ehrlich, L. Goerigk, Effect of the damping function in dispersion corrected density functional theory, *J. Comput. Chem.* 32 (7) (2011) 1456–1465.
- [51] A.V. Marenich, C.J. Cramer, D.G. Truhlar, Universal Solvation Model Based on Solute Electron Density and on a Continuum Model of the Solvent Defined by the Bulk Dielectric Constant and Atomic Surface Tensions, *J. Phys. Chem. B* 113 (18) (2009) 6378–6396.
- [52] Gaussian 16, R.C., Frisch, M. J., et al., Gaussian, Inc. 2016: Wallingford CT.
- [53] R. Hernández-Esparza, et al., GPUs as boosters to analyze scalar and vector fields in quantum chemistry, *Int. J. Quantum Chem.* 119 (2) (2019) e25671.
- [54] W. Humphrey, A. Dalke, K. Schulten, VMD: Visual molecular dynamics, *J. Mol. Graph.* 14 (1) (1996) 33–38.
- [55] L. Kalé, et al., NAMD2: Greater Scalability for Parallel Molecular Dynamics, *J. Comput. Phys.* 151 (1) (1999) 283–312.
- [56] L.S. Dodda, et al., 1.14*CM1A-LBCC: Localized Bond-Charge Corrected CM1A Charges for Condensed-Phase Simulations, *J. Phys. Chem. B* 121 (15) (2017) 3864–3870.
- [57] L.S. Dodda, et al., LigParGen web server: an automatic OPLS-AA parameter generator for organic ligands, *Nucleic Acids Res.* 45 (W1) (2017) W331–W336.
- [58] J. Huang, A.D. MacKerell Jr, CHARMM36 all-atom additive protein force field: Validation based on comparison to NMR data, *J. Comput. Chem.* 34 (25) (2013) 2135–2145.
- [59] T.A. Halgren, Merck molecular force field. I. Basis, form, scope, parameterization, and performance of MMFF94, *J. Comput. Chem.* 17 (5–6) (1996) 490–519.
- [60] L. Martínez, et al., PACKMOL: A package for building initial configurations for molecular dynamics simulations, *J. Comput. Chem.* 30 (13) (2009) 2157–2164.
- [61] S.J. Marrink, et al., The MARTINI Force Field: Coarse Grained Model for Biomolecular Simulations, *J. Phys. Chem. B* 111 (27) (2007) 7812–7824.
- [62] S. Kaur, A. Yethiraj, Chemically realistic coarse-grained models for polyelectrolyte solutions, *J. Chem. Phys.* 156 (9) (2022) 094902.
- [63] S. Mantha, A. Yethiraj, Conformational Properties of Sodium Polystyrenesulfonate in Water: Insights from a Coarse-Grained Model with Explicit Solvent, *J. Phys. Chem. B* 119 (34) (2015) 11010–11018.
- [64] B.L. Bouzo, et al., In Vitro–In Silico Modeling Approach to Rationally Designed Simple and Versatile Drug Delivery Systems, *J. Phys. Chem. B* 124 (28) (2020) 5788–5800.
- [65] T. Bereau, K. Kremer, Automated Parametrization of the Coarse-Grained Martini Force Field for Small Organic Molecules, *J. Chem. Theory Comput.* 11 (6) (2015) 2783–2791.
- [66] S.E. Feller, et al., Constant pressure molecular dynamics simulation: The Langevin piston method, *J. Chem. Phys.* 103 (11) (1995) 4613–4621.
- [67] S. Luo, et al., A Stopped-Flow Kinetic Study of the Assembly of Interpolymer Complexes via Hydrogen-Bonding Interactions, *Macromolecules* 39 (13) (2006) 4517–4525.
- [68] Y. Zhang, et al., DDSolver: An Add-In Program for Modeling and Comparison of Drug Dissolution Profiles, *AAPS J.* 12 (3) (2010) 263–271.
- [69] J. Catalan-Figueroa, et al., A mechanistic approach for the optimization of loperamide loaded nanocarriers characterization: Diafiltration and mathematical modeling advantages, *Eur. J. Pharm. Sci.* 125 (2018) 215–222.
- [70] L. Nothnagel, M.G. Wacker, How to measure release from nanosized carriers? *Eur. J. Pharm. Sci.* 120 (2018) 199–211.
- [71] I. Moreno-Villoslada, et al., Comparative Study of the Self-Aggregation of Rhodamine 6G in the Presence of Poly(sodium 4-styrenesulfonate), Poly(N-phenylmaleimide-co-acrylic acid), Poly(styrene-alt-maleic acid), and Poly (sodium acrylate), *J. Phys. Chem. B* 114 (37) (2010) 11983–11992.
- [72] I. Moreno-Villoslada, et al., π -Stacking of rhodamine B onto water-soluble polymers containing aromatic groups, *Polymer* 47 (19) (2006) 6496–6500.
- [73] H. Sun, et al., The π - π Stacked Geometries and Association Thermodynamics of Quinacridone Derivatives Studied by 1H NMR, *Chem. A Eur. J.* 110 (37) (2006) 10750–10756.
- [74] F. Parenti, et al., π -Stacking Signature in NMR Solution Spectra of Thiophene-Based Conjugated Polymers, *ACS Omega* 2 (9) (2017) 5775–5784.
- [75] H.R. Masoodi, S. Bagheri, Interplay between π - π stacking and cation- π interaction: a theoretical NMR study, *J. Iran. Chem. Soc.* 12 (10) (2015) 1883–1892.
- [76] L. Zhao, H. Zhang, W. Wang, π - π stacking interaction in mixed surfactant solutions assembled by cationic surfactant and organic salt with a naphthalene nucleus, *J. Mol. Liq.* 240 (2017) 14–20.
- [77] H. Nageh, Y. Wang, T. Nakano, Cationic polymerization of dibenzofulvene leading to a π -stacked polymer, *Polymer* 144 (2018) 51–56.
- [78] A.S. Mitchell, M.A. Spackman, Molecular surfaces from the promolecule: A comparison with Hartree-Fock ab initio electron density surfaces, *J. Comput. Chem.* 21 (11) (2000) 933–942.
- [79] H. Sato, H. Seki, Kinetic Study on the Formation of Polyelectrolyte Complexes. Poly(L-lysine hydrobromide) and Poly(L-glutamate sodium salt), *Polym. J.* 25 (5) (1993) 529–533.
- [80] Z. Zhu, S.P. Armes, S. Liu, pH-Induced Micellization Kinetics of ABC Triblock Copolymers Measured by Stopped-Flow Light Scattering, *Macromolecules* 38 (23) (2005) 9803–9812.
- [81] J. Zhang, et al., Stopped-flow kinetic studies of the formation and disintegration of polyion complex micelles in aqueous solution, *PCCP* 16 (1) (2014) 117–127.
- [82] S. Tian, et al., pH-Regulated Reversible Transition Between Polyion Complexes (PIC) and Hydrogen-Bonding Complexes (HBC) with Tunable Aggregation-Induced Emission, *ACS Appl. Mater. Interfaces* 8 (6) (2016) 3693–3702.
- [83] F.E. Agrò, M. Vennari, Physiology of Body Fluid Compartments and Body Fluid Movements, in: F.E. Agrò (Ed.), *Body Fluid Management: from Physiology to Therapy*, Springer Milan, Milano, 2013, pp. 1–25.
- [84] Brinkman, J.E., B. Dorius, and S. Sharma, *Physiology, Body Fluids*, in *StatPearls*. 2023, StatPearls Publishing Copyright © 2023, StatPearls Publishing LLC.: Treasure Island (FL).
- [85] Drugs to prevent COVID-19: living guideline. 2021: <https://app.magicapp.org/#/guideline/L6RxyL>.
- [86] X. Wang, et al., Scale-up of microreactor: Effects of hydrodynamic diameter on liquid-liquid flow and mass transfer, *Chem. Eng. Sci.* 226 (2020) 115838.
- [87] D.S. Duarte, J.A.d.A. Nascimento, D.d. Britto, Scale-up in the synthesis of nanoparticles for encapsulation of agroindustrial active principles, *Ciência e Agrotecnologia* (2019) 43.
- [88] M. Hanif, et al., Pharmacological basis for the medicinal use of Alcea rosea in airways disorders and chemical characterization of its fixed oils through GC-MS, *Pak J Pharm Sci* 32 (5(Supplementary)) (2019) 2347–2355.
- [89] S.J. Paluck, T.H. Nguyen, H.D. Maynard, Heparin-Mimicking Polymers: Synthesis and Biological Applications, *Biomacromolecules* 17 (11) (2016) 3417–3440.
- [90] Rahman, S. and R. Marathi, Sodium Polystyrene Sulfonate, in *StatPearls*. 2023, StatPearls Publishing Copyright © 2023, StatPearls Publishing LLC.: Treasure Island (FL).

- [91] R. Singh, J.W. Lillard Jr., Nanoparticle-based targeted drug delivery, *Exp Mol Pathol* 86 (3) (2009) 215–223.
- [92] W.R. Zhuang, et al., Applications of π - π stacking interactions in the design of drug-delivery systems, *J Control Release* 294 (2019) 311–326.
- [93] Y. Shi, et al., Π - Π Stacking Increases the Stability and Loading Capacity of Thermosensitive Polymeric Micelles for Chemotherapeutic Drugs, *Biomacromolecules* 14 (6) (2013) 1826–1837.
- [94] M.C. Childers, V. Daggett, Validating Molecular Dynamics Simulations against Experimental Observables in Light of Underlying Conformational Ensembles, *J. Phys. Chem. B* 122 (26) (2018) 6673–6689.
- [95] O.M.H. Salo-Ahen, et al., Molecular Dynamics Simulations in Drug Discovery and Pharmaceutical Development, *Processes* 9 (2021), <https://doi.org/10.3390/pr9010071>.
- [96] N. Farhadian, et al., Molecular dynamics simulation of drug delivery across the cell membrane by applying gold nanoparticle carrier: Flutamide as hydrophobic and glutathione as hydrophilic drugs as the case studies, *J. Mol. Graph. Model.* 116 (2022) 108271.
- [97] A. Bunker, T. Róg, Mechanistic Understanding From Molecular Dynamics Simulation in Pharmaceutical Research 1: Drug Delivery, *Front. Mol. Biosci.* 7 (2020).
- [98] X. Xu, et al., Application of molecular dynamics simulation in self-assembled cancer nanomedicine, *Biomaterials Research* 27 (1) (2023) 39.
- [99] A. de Barros, et al., Polymeric nanoparticles and nanomicelles of hydroxychloroquine co-loaded with azithromycin potentiate anti-SARS-CoV-2 effect, *J Nanostructure Chem* 13 (2) (2023) 263–281.
- [100] P. Urbán, et al., Use of poly(amidoamine) drug conjugates for the delivery of antimalarials to Plasmodium, *J Control Release* 177 (2014) 84–95.
- [101] E. Martí Coma-Cros, et al., Polyamidoamine Nanoparticles for the Oral Administration of Antimalarial Drugs, *Pharmaceutics* 10 (2018), <https://doi.org/10.3390/pharmaceutics10040225>.
- [102] A. Kashyap, et al., Chloroquine diphosphate bearing dextran nanoparticles augmented drug delivery and overwhelmed drug resistance in Plasmodium falciparum parasites, *Int. J. Biol. Macromol.* 114 (2018) 161–168.
- [103] S. Tripathy, et al., Synthesis, characterization of chitosan-tripolyphosphate conjugated chloroquine nanoparticle and its in vivo anti-malarial efficacy against rodent parasite: a dose and duration dependent approach, *Int J Pharm* 434 (1–2) (2012) 292–305.
- [104] S. Tripathy, et al., A prospective strategy to restore the tissue damage in malaria infection: Approach with chitosan-trypolyphosphate conjugated nanochloroquine in Swiss mice, *Eur. J. Pharmacol.* 737 (2014) 11–21.
- [105] S. Tripathy, et al., A novel chitosan based antimalarial drug delivery against Plasmodium berghei infection, *Acta Trop* 128 (3) (2013) 494–503.
- [106] S. Tripathy, et al., The Impact of Nanochloroquine on Restoration of Hepatic and Splenic Mitochondrial Damage against Rodent Malaria, *Journal of Nanoparticles* 2013 (2013) 106152.
- [107] G.A. Magalhães Jr, et al., Chitosan/Sterculia striata polysaccharides nanocomplex as a potential chloroquine drug release device, *Int. J. Biol. Macromol.* 88 (2016) 244–253.
- [108] H. Shafi, et al., Dehydroascorbate-derivatized chitosan particles for targeting antimalarial agents to infected erythrocytes, *Int J Pharm* 524 (1–2) (2017) 205–214.
- [109] M. Usman, M. Akhyar Farrukh, Delayed release profile of iron nano-chloroquine phosphate and evaluation of its toxicity, *Mater. Today: Proc.* 5 (7, Part 3) (2018) 15645–15652.
- [110] A.K. Bajpai, J. Choubey, Design of gelatin nanoparticles as swelling controlled delivery system for chloroquine phosphate, *J. Mater. Sci. - Mater. Med.* 17 (4) (2006) 345–358.
- [111] T.L. Lima, et al., Improving Encapsulation of Hydrophilic Chloroquine Diphosphate into Biodegradable Nanoparticles: A Promising Approach against Herpes Virus Simplex-1 Infection, *Pharmaceutics* 10 (2018), <https://doi.org/10.3390/pharmaceutics10040255>.
- [112] J.-H. Sun, et al., Co-delivery nanoparticles of doxorubicin and chloroquine for improving the anti-cancer effect in vitro, *Nanotechnology* 30 (8) (2019) 085101.
- [113] X. Zhang, et al., The chemotherapeutic potential of PEG-b-PLGA copolymer micelles that combine chloroquine as autophagy inhibitor and docetaxel as an anti-cancer drug, *Biomaterials* 35 (33) (2014) 9144–9154.
- [114] Y. Yang, et al., Micelle nanovehicles for co-delivery of Lepidium meyenii Walp. (maca) polysaccharide and chloroquine to tumor-associated macrophages for synergistic cancer immunotherapy, *Int. J. Biol. Macromol.* 189 (2021) 577–589.
- [115] M.R. Bhalekar, P.G. Upadhaya, A.R. Madgulkar, Fabrication and efficacy evaluation of chloroquine nanoparticles in CFA-induced arthritic rats using TNF- α ELISA, *Eur. J. Pharm. Sci.* 84 (2016) 1–8.
- [116] J.O. Muga, et al., In vitro evaluation of chloroquine-loaded and heparin surface-functionalized solid lipid nanoparticles, *Malar. J.* 17 (1) (2018) 133.